

ISSN 2071-3592

童綜合醫學雜誌

Tungs' Medical Journal



Volume 7 Number 2 December 2013

TUNGS' MEDICAL JOURNAL

Publisher: Jai-Nien Tung

Editor-in-Chief: Tzu-Ming Chang

Editorial Consultant: Yin-Chung Chen Jue-Hawn Yin

Associate Editors: Ching-Shiang Chi Hung-Yi Hsu Wen-Jinn Liaw
Jui-Wen Tung

Executive Editors: Shung-Sheng Tsou

Editors:

Yu-Chun Yin	Jia-Yi Wang	Ka-Sic Ho	Hsiu-Fen Lee
Huei-Jane Lee	Paik-Seong Lin	Chen-Wei Lin	Jing-jHeng Lin
Chao-Tang Lin	Jong-Shiaw Jin	Jyh-Cherng Yu	Dai-Lung Char
Jen-Huey Chiang	Shao-Keh Hsu	Tsung-Ming Chen	Pei-Liang Chen
Der-Yuan Chen	Tang-Yi Tsao	Chin-Jen Tseng	Min-Che Tung
Jui-Fen Huang	Kun-Tu Yeh	Ting-Yu Yeh	Pin-Ho Pan
Chin-Shaw Tsai	Kee-Ching Jeng	Kim Seng Law	Shing-Hwa Lu

Liang-Po Hsieh

Statistical consultant: Ya-Chung Jeng

Legal Consultant: Sung-Hu Lin Ching-Bin Huang

Editorial Assistants: Meng-I Wang Mei-Hui I

Editorial Office:

The Tungs' Medical Journal, Tungs' Taichung MetroHarbor Hospital.

No.699, Sec. 8, Taiwan Blvd., Wuqi Dist., Taichung City 43503, Taiwan (R.O.C.)

E-Mail: Tungs_Journal@ms.sltung.com.tw

Tel.: 886-4-26581919 ext. 58047 Fax: 886-4-26582193

Printing Company:

Great C Printing Co.

Tel: 886-2-2302-3939 Fax: 886-2-2302-2036

Tungs' Medical Journal

CONTENTS IN BRIEF

REVIEW ARTICLE

- 37 **Clinical Trials of Antiangiogenic Agents in Epithelial Ovarian Cancer: A Review**
Kim Seng Law

ORIGINAL ARTICLE

- 44 **Diagnostic Performance in Differentiating Colorectal polyps: Narrow Band Image and Conventional White Light Image**
Ming-Hung Tsai, Wei-Chih Shen
- 59 **Apple Polyphenol Inhibits Lipopolysaccharide-induced Inflammation in an Animal Model**
Huei-Jane Lee

CASE REPORT

- 66 **Transient Oxygen Desaturation During Removal of A Huge Ovarian Tumor Under Intubated General Anesthesia: A Case Report**
Yiu-Sion Chen, Kuo-Sheng Huang, Kam-Sun Cheung, Kee-Ming Man, Chun-Lai Ma, Chen-Lung Chien
- 70 **Tophaceous Gout of the Lumbar Spine: A case report**
Hsin-Pai Lee, Se-Yuan Liu, Shih-Peng Hsieh, Cherng-Gueih Shy, Yen-Hsuan Jean
- 76 **Case Report of Magnetic Resonance Imaging Findings Japanese Encephalitis**
Chung-Chih Kao, Chia-Ru Li, Ching-Shiang Chi, Ai-Min KuLiu, Stella Chin-Shaw Tsai, Chia-Hui Kao

Review Article

Clinical Trials of Antiangiogenic Agents in Epithelial Ovarian Cancer: A Review

Kim Seng Law*

Department of Obstetrics and Gynecology/ Cancer Center Tungs' Taichung MetroHarbor Hospital

Received: Jan. 14, 2014; Accepted: Jan. 23, 2014

Abstract

Angiogenesis plays a vital role in the development of tumor progression and metastasis as well as ascitic formation. Several clinical trials with agents targeting the specific angiogenic factors such as the vascular epithelial growth factors (VEGF), vascular epithelial growth factor receptor (VEGFR), platelets-derived growth factors (PDGF) and fibroblast-derived growth factors (FDGF) has gained major progression in the setting of adjuvant and maintenance treatment of epithelial ovarian cancer. We summarize the clinical trials of the antiangiogenic agents with focusing on the primary end points as well as the secondary end points in the primary as well as recurrent settings and discuss the benefits and probable limitations of this agents in the treatment of epithelial ovarian cancer.

Key words: Angiogenesis, Epithelial Ovarian Cancer Vascular epithelial growth factor

Epithelial ovarian cancer (EOC) has the highest mortality among gynecological cancers in the United States^[1], with almost 75% of the disease occurring at the advanced stage^[2]. Despite aggressive surgical interventions and novel chemotherapeutic agents, there was only a limited improvement in the 5-year survival of patients with ovarian cancer during the past decades, i.e., from 37% in 1975–1977 to 46% in 1999–2005^[3].

The standard treatment for EOC involves either a primary debulking surgery followed by six cycles of platinum-based chemotherapy or three cycles of neoadjuvant chemotherapy (NACT) in patients deemed to have suboptimal probability of surgical success (>1 cm residual tumor) followed by another three cycles of platinum-based adjuvant chemotherapy^[4,5]. Although different routes and schedules of chemotherapy delivery have resulted in a slight improvement in the survival of patients with

advanced disease^[6,7,8,9], there remains an urgent need for more effective treatments.

Tumor angiogenesis is an essential component of cancer growth and metastasis. It is mediated by key angiogenic molecules such as the vascular endothelial growth factor (VEGF) and its two receptors: VEGF receptor-1 (Flt-1) and VEGF-2 (KDR). VEGF and VEGF receptors are expressed in EOC; moreover, increased VEGF expression has been associated with the development of malignant ascites^[10,11,12]. Other angiogenesis pathways involved in the pathogenesis of ovarian cancer include platelet-derived growth factor (PDGF) and fibroblast growth factor (FGF). Higher PDGF levels have been observed in ovarian carcinomas than in benign tissue and malignant ascites, and have been linked to poor survival; evidence has shown similar involvement of the FGF pathway in ovarian angiogenesis^[13,14,15].

Of the antiangiogenic agents being evaluated^[18,19,20], bevacizumab (Avastin; Genentech, South San Francisco, CA, USA) is the most widely studied. In a phase II trial in patients with untreated stage >IC EOC, primary peritoneal cancer (PPC), fallopian tube cancer (FTC), or uterine papillary serous

*Correspondence to: Kim Seng Law, Department of Obstetrics and Gynecology/ Cancer Center Tungs' Taichung MetroHarbor Hospital. No.699, Sec.8, Taiwan Blvd., Wuqi Dist., Taichung City 43503, Taiwan (R.O.C.)

carcinomas, the overall response rate was 75% with a median progression-free survival (PFS) of 29.8 months^[21]. This result has led to a phase III trial—Gynecologic Oncology Group (GOG) 218 study.

Here we present the most recent results of clinical trials regarding the utility of antiangiogenic agents in the treatment of epithelial ovarian cancer.

Front line settings

GOG 218

In the GOG 218 study, the effect bevacizumab was assessed in patients with stage III and IV EOC; bevacizumab was administered at the dose of 15 mg/kg every 3 weeks for up to 15 months. The trial consisted of three treatment arms: (a) standard intravenous paclitaxel and carboplatin, (b) intravenous paclitaxel and carboplatin in conjunction with bevacizumab, and (c) intravenous paclitaxel, carboplatin, and bevacizumab with continuation of bevacizumab as a single agent for an additional 10 months as maintenance therapy.

The main finding of the study was a significantly improved PFS of 3.8 months when bevacizumab was administered concurrently with chemotherapy and continued as maintenance therapy. An overall survival (OS) benefit was not evident in GOG 218. Nonetheless, because 40% of patients in the chemotherapy-only group subsequently received bevacizumab at progression, a potential OS benefit would have been difficult to demonstrate in this study^[22].

ICON7

This is a phase III, open label, Medical Research Council -sponsored academia-led Roche-supported trial to evaluate the use of bevacizumab and to support a front line ovarian cancer filing with the European Medical Agency (EMA).

A total of 1,528 patients were given carboplatin (AUC 5 or 6) and paclitaxel 175 mg/m² every 3 weeks for 6 cycles with or without bevacizumab. Bevacizumab (7.5 mg/kg) was concurrently administered every 3 weeks for 6 cycles and continued for an additional 12 cycles or until disease progression. Interim analysis of the ICON-7 study showed an overall PFS advantage for patients receiving bevacizumab for 2.4 months at all stages (FIGO stage I–IV). In the high-risk group (suboptimally debulked stage

III residual disease, i.e., tumor size >1 cm, or stage IV), a median OS benefit of approximately 8 months was seen with bevacizumab [hazard ratio (HR), 0.64, $P = 0.002$]^[23]. The final data of the study revealed that the median OS was 58 months and that bevacizumab-based therapy does not increase OS compared with placebo. On the other hand, a benefit of 9.4 months in median survival time was observed in the patients at high risk of progression. Thus, some women with high-risk disease may benefit from bevacizumab.

OCTAVIA

This was a single-arm, phase II front-line study evaluating bevacizumab with weekly paclitaxel and every 3 weeks of carboplatin, followed by bevacizumab maintenance therapy for up to 1 year in patients with stage I/IIA (with grade 3 or clear cell histology) or stage IIB/IV disease of any grade. Overall, the safety profile of weekly paclitaxel in combination with bevacizumab and carboplatin was comparable to that observed in ICON7^[24].

AGO-OVAR12/LUME-Ovar

Nintedanib (BIBF 1120; Boehringer Ingelheim, Ingelheim, Germany) targets VEGFR-1, -2, and -3, PDGFR- α/β , FGFR-1, -2, and -3, members of the v-src sarcoma viral oncogene homolog (Src family), and fms-like tyrosine kinase 3 (Flt-3). In a phase II randomized controlled trial comparing nintedanib 250 mg twice daily with placebo as maintenance therapy in patients with recurrent EOC, PPC, or FTC who responded to their last chemotherapy regimen, the primary endpoint of 36-week PFS was 16.3% with nintedanib versus 5.0% with placebo (HR, 0.65; 95% CI, 0.42–1.02; $P = 0.06$), which led to the AGO-OVAR12/LUME-Ovar1 study, in which patients with EOC, PPC, or FTC were accrued for nintedanib combined with carboplatin/paclitaxel in first-line settings, followed by nintedanib maintenance therapy until disease progression or for a maximum of 120 weeks. The data on the primary endpoints of PFS is expected to come out in 2016.

AGO-OVAR16

Pazopanib (GlaxoSmithKline, London, UK) targets VEGFR-1, -2, and -3; PDGFR- α/β ; FGFR-1 and -3; and c-kit. In an open-label Phase II trial^[25] evaluating pazopanib 800 mg/day in patients with pretreated recurrent EOC or PPC with a complete cancer antigen

(CA)-125 response to initial platinum-based chemotherapy and subsequent CA-125 elevation to >42 U/mL. The primary endpoint of the CA-125 response was seen in 11 of 36 patients (31%; 95% CI, 16–48%).

AGO-OVAR16 is a randomized, double-blind, phase III trial (n = 940) to determine whether pazopanib 800 mg/day administered for up to 24 months prolongs PFS compared with placebo in women with nonbulky, FIGO stage II–IV ovarian cancer, which has not progressed after front-line chemotherapy. The data presented at the 2013 Meeting of the American Society of Clinical Oncology showed that pazopanib maintenance therapy significantly improved PFS (median 12.3 versus 17.9 months; HR = 0.766; $P = 0.0021$) with some class-specific adverse effects that led to early discontinuation and dose reductions.

TRINOVA-3

AMG 386 (Amgen; Thousand Oaks, CA, USA) is a peptide–Fc fusion protein that targets angiogenesis by inhibiting the binding of both angiopoietins-1 and -2 to Tie-2 receptor^[26]. Patients with stage III or IV disease with no prior anticancer or experimental therapy for EOC, PPC, or FTC prior primary debulking surgery within 12 weeks were randomized to receive first-line carboplatin/paclitaxel combined with AMG 386, followed by AMG 386 maintenance therapy for 18 months until disease progression. The study was initiated in December 2011, with the final data collection for the primary endpoint of PFS expected in 2016.

Recurrent settings

OCEANS

A total of 484 patients enrolled in a randomized, multicenter, blinded, placebo-controlled phase III trial testing the efficacy and safety of bevacizumab with gemcitabine and carboplatin compared with gemcitabine and carboplatin in platinum-sensitive recurrent EOC, PPC, or FTC for 6–10 cycles. Bevacizumab or placebo was then continued until disease progression. The primary endpoint was PFS by the Response Evaluation Criteria in Solid Tumors (RECIST); secondary endpoints were the objective response rate, duration of response, OS, and safety.

PFS in the bevacizumab arm was superior to that in the placebo arm (HR, 0.485; 95% CI, 0.388–0.605;

log-rank $P < 0.001$; median PFS 12.4 versus 8.4 months). The objective response rate (78.5% versus 57.4%; $P < 0.001$) and duration of response (10.4 versus 7.4 months; HR, 0.534; 95% CI, 0.408–0.698) significantly improved with the addition of bevacizumab^[27].

AURELIA

This is a randomized, 2-arm phase III trial to assess the efficacy and safety of bevacizumab in combination with a range of chemotherapy regimens (including paclitaxel, topotecan, and liposomal doxorubicin) in patients with platinum-resistant ovarian cancer. At median follow-up of >13 months, median PFS was significantly prolonged with chemotherapy plus bevacizumab versus chemotherapy alone (6.7 versus 3.4 months, respectively; HR, 0.48; 95% CI, 0.38–0.60; $P < 0.001$)^[28]. With median follow-up time of 27.4 months, 264 of 361 patients died. Bevacizumab improved median OS from 13.3 to 16.6 months compared with chemotherapy alone. Nevertheless, this survival benefit did not reach statistical significance. It is worth noting that the AURELIA trial did not have sufficient statistical power to detect a significant difference in OS, and the interpretation of OS was confounded by preplanned crossover at disease progression in the chemotherapy arm. A total of 40% of patients in the chemotherapy arm received bevacizumab after disease progression. A more pronounced OS benefit was observed in the cohort treated with paclitaxel (HR, 0.65; median 22.4 versus 13.2 months).

TRINOVA-1

This is a phase III, randomized, double-blind trial of weekly paclitaxel plus angiopoietin-1 and -2 inhibitor trebananib or placebo in women with recurrent ovarian cancer. A total of 919 patients were enrolled who fit the following criteria: partially platinum-sensitive or -resistant recurrent ovarian cancer, one prior front-line platinum-based regimen, and allowed to receive two additional cytotoxic regimens. The addition of trebananib significantly prolonged the primary endpoint of PFS from 5.4 to 7.2 months (HR, 0.66; $P < 0.001$). The response rate was 38% in the trebananib arm compared with 30% in the placebo arm. Preplanned interim analysis showed an overall favorable OS trend for trebananib, which was not statistically significant. The main toxicities observed in the trebananib arm were edema, pleural effusion,

and ascites. VEGF-associated adverse events such as hypertension, proteinuria, and arterial thrombotic events were not increased in this study.

TRINOVA-2

This study evaluated pegylated liposomal doxorubicin in combination with either placebo or AMG 386 in previously treated patients with EOC, PPC, or FTC who had <3 prior platinum-based chemotherapy regimens or who had a platinum-free interval of <12 months from the first platinum-based therapy. The study was initiated in March 2011 and is to be completed in April 2014.

TRINOVA-3

Patients with stage III or IV disease with no prior anticancer or experimental therapy for EOC, PPC, or FTC prior primary debulking surgery within 12 weeks were randomized to receive first-line carboplatin/paclitaxel combined with AMG 386, followed by AMG 386 maintenance therapy for 18 months until disease progression. The study was initiated in December 2011, with the final data collection for the primary endpoint of PFS expected in 2016.

ICON6

Cediranib (Recentin; AstraZeneca, Wilmington, DE, USA) is a tyrosine kinase inhibitor targeting VEGFR-1, -2, and -3; PDGFR; FGFR-1; and c-kit^[29]. The ICON6 trial evaluated the addition of 20 mg/day cediranib to platinum-based chemotherapy—concurrently with chemotherapy—with cediranib continued as a maintenance therapy for 18 months in patients with a first relapse of platinum-sensitive ovarian cancer. The restricted means analysis showed a statistically significant benefit in both PFS and OS in the cediranib maintenance arm although a higher discontinuation rate was reported with cediranib. The median OS in the control arm of ICON6 was shorter than that of the OCEANS study (20 versus 35 months). These data might imply that fewer patients received poststudy antiangiogenic therapy (39% in OCEANS, with no disclosure in ICON6).

Discussion

There has been no major breakthrough regarding the treatment outcome of advanced EOC in the past few decades. Optimized therapeutic

agents are urgently sought with the hope that one of them will delay or prevent recurrence in most cases of advanced-stage disease. With the advent of antiangiogenic drugs/biologics and the effectiveness demonstrated in PFS and marginal OS, it seems that the battle against EOC has finally come to a turning point.

Although antiangiogenic agents seem to be the most promising molecularly targeted therapeutics, some controversies have yet to be solved before large-scale clinical use is feasible.

First, the optimal dosage and duration of antiangiogenic agents remain to be elucidated, as seen in ICON7 and GOG 218, which used different doses (7.5 mg/kg and 15 mg/kg, respectively) and different durations of maintenance (18 cycles versus 15 cycles). In addition, the convergence of the PFS curves after the end of bevacizumab maintenance therapy raises the question of the appropriate duration of therapy. In ongoing trials concerning EOC, the duration of maintenance therapy is 24 months with pazopanib (AGO-OVAR16), approximately 60 weeks with cediranib (ICON6), 18 months with AMG 386 (TRINOVA-3), and approximately 24 months with nintedanib (AGO-OVAR12/LUME-Ovar I). The concept of administering these molecular agents until disease progression is an intriguing strategy, particularly when the risk of recurrence is high. A trial comparing first-line chemotherapy plus bevacizumab and maintenance of bevacizumab for 16 cycles versus 38 cycles is in progress (AGO-OVAR17 BOOST), and the results are eagerly anticipated.

Second, the question of optimal endpoints needs to be addressed. According to the GCIIG Fourth Cancer Consensus Conference, endpoints for front-line/maintenance clinical trials need to be specifically defined and may include PFS, OS, toxicity, and/or patient-reported outcomes^[30]. Although both PFS and OS are important, PFS is often the preferred primary endpoint owing to the confounding effects of subsequent therapy upon progression with OS.

Third, the timing of adding antiangiogenic agents needs to be clarified. Although both ICON7 and GOG 218 show benefits of adding bevacizumab to first-line chemotherapy and as maintenance therapy, neither trial compared this approach with maintenance therapy alone. In the same way, TRINOVA-3 is evaluating AMG 386 in combination with carboplatin/paclitaxel followed by AMG 386 maintenance, the

AGO-OVAR12/LUME-Ovar I is evaluating nintedanib in combination with carboplatin/paclitaxel as a maintenance therapy, and ICON6 also includes concurrent cediranib in the chemotherapy arm. The effects of antiangiogenic agents in the settings of neoadjuvant therapy and withholding the agents until complete clinical remission is an interesting field and warrants further studies.

Finally, because the PDGF and FGF signaling pathways appear to be involved in VEGF resistance described across various solid tumors, combination inhibition of VEGF and PDGF and/or FGF may inhibit angiogenesis more strongly than VEGF inhibition alone. These data have led to phase II trials of temsirolimus (targeting mTOR) plus bevacizumab and of other promising combinations of novel agents to be explored in the near future.

References

1. Robboy SL, Mutter GL, Prat I et al. Lacey JV, Sherman ME. Ovarian neoplasia. In: Robboy's Pathology of the Female Reproductive Tract, 2 nd ed. Churchill Livingstone Elsevier, Oxford 2009;601.
2. FIGO staging classifications and clinical practice guidelines in the management of gynecologic cancers. *Int J Gynecol Obstet* 2000;70:209-62
3. Jemal A, Siegel R, Xu J, Ward E. *Cancer Statistics, 2010*. *CA Cancer J Clin* 2010;60(5):277-300.
4. Boente MP, Chi DS. The role of surgery in the management of ovarian cancer: primary and interval cytoreductive surgery. *Hoskins WJSO Semin Oncol*. 1998;25(3):326.
5. Vergote I, TropéCG, Amant F, Kristensen GB, Ehlen T, Johnson N, et al. Neoadjuvant chemotherapy or primary surgery in stage IIIc or IV ovarian cancer. European Organization for Research and Treatment of Cancer-Gynaecological Cancer Group, NCIC Clinical Trials GroupSON Engl J Med. 2010;363(10):943.
6. Armstrong DK, Bundy B, Wenzel L, Huang HQ, Baergen R, Lele S, et al. Intraperitoneal cisplatin and paclitaxel in ovarian cancer. *Gynecologic Oncology GroupSON Engl J Med*. 2006;354(1):34.
7. Markman M, Bundy BN, Alberts DS, Fowler JM, Clark-Pearson DL, Carson LF, et al. Phase III trial of standard-dose intravenous cisplatin plus paclitaxel versus moderately high-dose carboplatin followed by intravenous paclitaxel and intraperitoneal cisplatin in small-volume stage III ovarian carcinoma: an intergroup study of the Gynecologic Oncology Group, Southwestern Oncology Group, and Eastern Cooperative Oncology Group. *Sickel JSOJ Clin Oncol*. 2001;19(4):1001.
8. Katsumata N, Yasuda M, Takahashi F, Isonishi S, Jobo T, Aoki D, et al. Dose-dense paclitaxel once a week in combination with carboplatin every 3 weeks for advanced ovarian cancer: a phase 3, open-label, randomised controlled trial. *Japanese Gynecologic Oncology GroupSO Lancet*. 2009; 374(9698):1331.
9. Katsumata N, Yasuda M, Isonishi S, Takahashi F, Michimae H, Kimura E, et al. Long-term results of dose-dense paclitaxel and carboplatin versus conventional paclitaxel and carboplatin for treatment of advanced epithelial ovarian, fallopian tube, or primary peritoneal cancer (JGOG 3016): a randomised, controlled, open-label trial. *Japanese Gynecologic Oncology Group SO Lancet Oncol*. 2013;14(10): 1020.
10. Ramakrishnan S, Subramanian IV, Yokoyama Y, Geller M. Angiogenesis in normal and neoplastic ovaries. *Angiogenesis* 2005;8:169-82.
11. Chen H, Ye D, Xie X, Chen B, Lu W. VEGF, VEGFRs expressions and activated STATs in ovarian epithelial carcinoma. *Gynecologic Oncology* 2004;94:630-5.
12. Santin AD, Hermonat PL, Ravaggi A, Cannn MJ, Pecorelli S, Parham GP. Secretion of vascular endothelial growth factor in ovarian cancer. *European Journal of Gynecological Oncology* 1999;20:177-81.
13. Dabrow MB, Francesco MR, McBrearty FX Caradonna S. The effects of platelet-derived growth factor and activated receptor on normal and neoplastic human ovarian surface epithelium. *Gynecologic Oncology* 1998;71:29-37.
14. Henriksen R, funa K, Wilander E, Backstrom T, Ridderheim M, Oberg K. Expression and prognostic significance of platelet-derived growth factor and its receptors in epithelial ovarian neoplasms. *Cancer Research* 1993;53:4550-4.
15. Matei D, Kelich S, Cao L et al. PDGFsecretion in ovarian cancer. *Cancer Biology and Therapy* 2007;6:1951-9.
16. Crickard K, Gross JL, Crickard U, et al. Basic fibroblast growth factor and receptor expression in human ovarian cancer. *Gynecologic Oncology* 1994;55:277-84.
17. Valve E, Martikainen P, Seppanen J Oksjoki et al. Expression of fibroblast growth factor-2 activity by human ovarian cancer tumor endometrium. *Clinical Cancer Research* 2005;11:4282-8.
18. Mabuchi S, Terai Y, Morishige K, et al. Maintenance treatment with bevacizumab prolongs survival in an in vivo ovarian cancer model. *Clinical Cancer research* 2008;14: 7781-9.
19. Burger RA, Sill MW, Monk BJ, Greer BE, Sorosky JI. Phase II trial of bevacizumab in persistent or recurrent epithelial ovarian cancer or primary peritoneal cancer: a Gynecologic Oncology Group Study. *Journal of Clinical Oncology* 2007;25:5165-71.
20. Cannistra SA, Matulonis UA, Penson RT, et al. Phase II study of bevacizumab in patients with platinum-resistant ovarian cancer or peritoneal serous cancer. *Journal of Clinical Oncology* 2007;25:5180-6.
21. Penson RT, Dizon DS, Cannistra SA, et al. Phase II study of carboplatin, paclitaxel, and bevacizumab with maintenance bevacizumab as first-line chemotherapy for advanced mullerian tumors. *Journal of Clinical Oncology* 2010;28:154-9.
22. Burger RA, Brady MF, Bookman MA, et al. Incorporation of bevacizumab in the primary treatment of ovarian cancer. *New England Journal of Medicine* 2011;365:2473-83.
23. Perren TJ, Swart AM, Pfisterer J, et al. A phase 3 trial of bevacizumab in ovarian cancer. *New England Journal of Medicine* 2011;365:2484-96.
24. Gonzalez-Martin A, Gladiëff L, Tholander B et al. Safety of front-line bevacizumab combined with weekly paclitaxel (wPAC) and q3w carboplatin(C) for ovarian cancer: Result from OCTAVIA. *Journal of Clinical Oncology* 2012;30.
25. Friedlander M, Hancock KC, Rischin D, et al. A phase II, open-label study evaluating pazopabnib in patients with

- recurrent ovarian cancer. *Gynecologic Oncology* 2010; 119;32-7.
26. Coxon A, Bready J, Min H, et al. Context-dependent role of angiotensin-1 inhibition in the suppression of angiogenesis and tumor growth: implications for AMG386, an angiotensin-1/2-neutralizing peptidomimetic. *Molecular Cancer Therapy* 2010;9:2641-51.
 27. Aghajanian C, Blank S, Goff B, Judson P, Teneriello M, Husain A, Sovak M et al. OCEANS: A randomized, double-blind, placebo-controlled phase III trial of chemotherapy with or without bevacizumab in patients with platinum-sensitive recurrent epithelial ovarian, primary peritoneal, or fallopian tube cancer. *Journal of Clinical Oncology* 2012.
 28. Pujade-Lauraine E, Hilpert F, Weber B, et al. AURELIA: A randomized phase III trial evaluating bevacizumab (BEV) plus chemotherapy (CT) for platinum (PT)-resistant recurrent ovarian cancer (OC). *J Clin Oncol* 30, 2012 (suppl; abstr LBA5002^).
 29. Lindsay CR, MacPherson GE, Cassidy J. Current status of cediranib: the rapid development of a novel anti-angiogenic therapy. *Future Oncology* 2009;5:421-35.
 30. Stuart GC, Kitchener H, Bacon M et al. 2010 Gynecologic Cancer InterGroup (GCIg) consensus statement on clinical trials in ovarian cancer: report from the Fourth Ovarian Cancer Consensus Conference. *International Journal of Gynecological Cancer* 2011;21:750-5.

抗血管新生藥物在卵巢上皮癌的臨床實驗回顧

劉錦成*

童綜合醫療社團法人 童綜合醫院 癌症中心/婦產科

受文日期：民國 103 年 1 月 14 日；接受刊載：民國 103 年 1 月 23 日

摘要

新生血管在腫瘤惡化，轉移以及腹水的形成上扮演了關鍵性的角色。臨床實驗上針對特定血管新生因子如血管上皮生長因子，血管上皮生長因子接受體，血小板相關生長因子，纖維細胞相關生長因子而研發出來的藥物在治療卵巢上皮癌時無論是應用在輔助性或維持性治療上都有著長足的進步。

我們針對抗血管新生因子藥物的臨床實驗在治療卵巢上皮癌不論是初始或復發情境下的主要以及次要臨床指標作了一整理，也探討了此藥物在治療上的好處以及可能的缺失。

關鍵詞：血管新生、卵巢上皮癌生長因子

Diagnostic Performance in Differentiating Colorectal polyps: Narrow Band Image and Conventional White Light Image

Ming-Hung Tsai¹, Wei-Chih Shen^{2*}

¹Division of Gastroenterology, Department of Medicine, Tungs' Taichung MetroHarbor Hospital

²Department of Computer Science and Information Engineering, Asia University, Taichung, Taiwan

Received: Mar. 28, 2013; Accepted: Nov. 27, 2013

Abstract

A majority of colon and rectal cancers arise from previously benign adenomas through the adenoma–carcinoma sequence. Discrimination between neoplastic and nonneoplastic lesions is crucial to avoid the overtreatment of nonneoplastic lesions. Narrow-band imaging (NBI) is a newly developed optical chromoendoscopy technique that highlights the microvascular structure of the mucosal surface without the inconvenience of dye spraying that is used in conventional chromoendoscopy. Both conventional chromoendoscopy and NBI utilize magnifying colonoscopy technology to achieve high diagnostic accuracy; however, magnifying colonoscopies are not routinely used in clinical practice. We analyzed the numerical data of the red, green, and blue components under white light (WL) and NBI in 36 polyps. Significant differences between two lesions were compared on the basis of various characteristics, including standard deviation (*SD*), *Kurt*, *Entropy*, and *Energy* for each component under WL and NBI; however, *SD* and *Kurt* were omitted for the red component under NBI. A more homogeneous mucosal surface on a hyperplastic polyp contributes to the presentation. In addition, the *mean* of the green component under NBI achieved a significant difference that may have resulted from less absorption over the larger pit area in an adenomatous polyp. The accuracy of the computer-aided diagnostic performance was higher for NBI than for WL; this was compatible with previous results from other clinical studies that did not use computer-aided analysis.

Key words: narrow-band imaging (NBI); white light (WL); colorectal polyps; computer-aided analysis

Introduction

It is generally accepted that a majority of colon and rectal cancers arise from previously benign adenomas through the adenoma–carcinoma sequence^[1]. Early detection and subsequent removal of adenomatous polyps have been reported to decrease the mortality and incidence of colorectal cancers^[2]. Histologically, polyps are classified as either neoplastic lesions (adenoma, adenocarcinoma) or nonneoplastic lesions. A majority of nonneoplastic polyps are hyperplastic polyps with no malignant potential; however, sessile serrated lesions that may be difficult to microscopically differentiate from

hyperplastic polyps are considered as precursors of microsatellite unstable cancers^[3]. Polypectomy or biopsy of a polyp for histopathological diagnosis is considered the gold standard for distinguishing between adenomatous and hyperplastic polyps. If we can confidently differentiate between these, risks associated with overtreatment of hyperplasia polyps can be avoided. However, the accuracy of differentiation is low when using conventional colonoscopy^[4].

High quality images can improve diagnostic accuracy by enhancing the level of resolution and the contrast of images. Resolution denotes the capacity to present minute patterns and is determined on the basis of lens characteristics and the number of pixels in the charged coupled devices (CCD). Two primary types of diagnostic modalities are currently available to improve the level of resolution: the magnifying endoscope and the high resolution endoscope.

*Correspondence to: Wei-Chih Shen, Department of Computer Science and Information Engineering, Asia University, No. 500, Lioufeng Rd., Wufeng, Taichung 41354, Taiwan, (R.O.C.)

Magnifying endoscopes are equipped with an optical zooming apparatus that increases the level of magnification. The fine mucosal surface can be evaluated in detail using magnifying endoscopes^[5]. On the other hand, the high resolution endoscope (HRE) is a newer imaging modality that provides high quality images by using a higher number of pixels in CCD than in conventional endoscopes^[5].

Conventional colonoscopy uses white light from a xenon source for its tissue illumination. Standard white light covers the full visible red–green–blue wavelength range (400–700 nm). The broadband, white-light illumination enables the endoscopist to observe lesions in natural light. When we use conventional colonoscopes, colon polyps are recognized as neoplastic lesions if reddish discoloration is present or if the lesion is more than 10 mm in size^[6]. Chromoendoscopy, which involves spraying dye over the mucosal surface, can improve the image of surface structures of mucosal lesions^[7-8]. Kudo et al. proposed the pit pattern for the classification of colonic polyps via magnifying chromoendoscopy which has a high degree of accuracy with regard to differentiation between two polyps^[9]. However, chromoendoscopy needs considerable time during the procedure for dye spraying and observation. Narrow-band imaging (NBI), also referred to as “optical chromoendoscopy,” utilizes optical interference filters that spectrally narrow the bandwidth of conventional white light into shorter wavelengths, as listed in Table 1. The shorter wavelength of light is within the absorption band for hemoglobin; images of the superficial vasculature and mucosal patterns on polyps can be improved. These changes are easily observed during endoscopy and are helpful to differentiate between abnormal and normal mucosa^[10-13].

The blue illumination, which is 415 nm in wavelength, corresponds to the first and main peak on the absorption spectrum of oxyhemoglobin. In addition, oxyhemoglobin demonstrates some absorption of green light, with a secondary peak at 540 nm. The NBI system takes advantage of these optical absorption characteristics at 415 nm of blue light and at 540 nm of green light to evaluate the mucosal surface. Currently available NBI systems use two narrow-band filters that provide tissue illumination in both of these spectrums of light. The image using blue light is sent to the blue image memory bank in the video processor. In addition, the same image is sent to the green image memory bank. The image below 540 nm is sent to the red image memory bank in the video processor. Therefore, the image using green illumination will be displayed as a red component image on the monitor. The 540-nm light penetrates deeply, and deep mucosal and submucosal vessels are emphasized. The image of capillaries in the superficial mucosal layer is strengthened by the 415-nm light.

A brown blob under low magnification is diagnosed as a neoplastic lesion in NBI^[4]. In an NBI image, the subepithelial microvascular architectures as well as mucosal microsurface structures are enhanced (Fig 1). Even during magnifying colonoscopy, meshed capillary vessels in normal colonic mucosa and

Table 1. The wave length used in the NBI system.

NBI system	NBI filter (bandwidth)	Image component
3-Band RGB	415 nm (30 nm)	Blue
	445 nm (60 nm)	Green
	500 nm (30 nm)	Red
2-Band RGB	415 nm (30 nm)	Blue and Green
	540 nm (20 nm)	Red

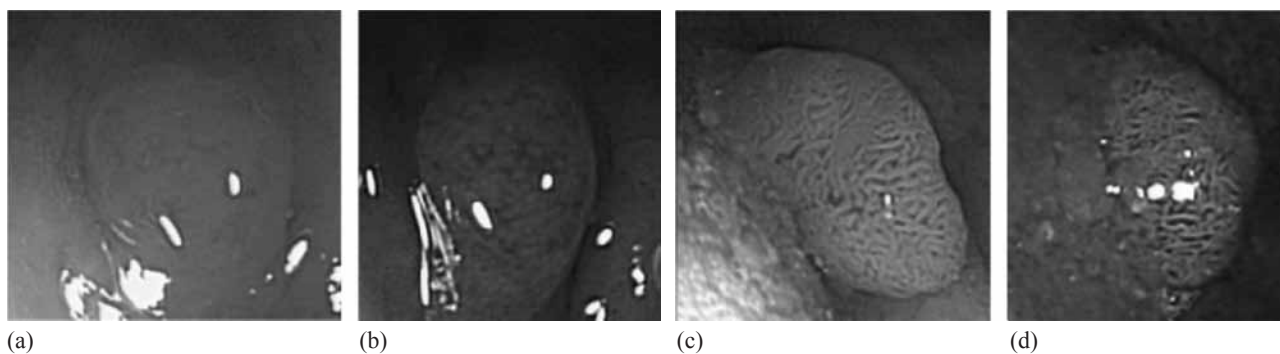


Fig. 1 (a) Non-magnified WL image of hyperplasia polyp; (b) Non-magnified NBI image of hyperplasia polyp; (c) Non-magnified WL image of adenomatous polyp; (d) Non-magnified NBI image of adenomatous polyp.

hyperplastic polyps are invisible or only faintly visible, and vessels on the surface of adenomatous polyps are clearly visible. Using magnifying NBI, a strong vascular pattern intensity (VPI) or meshed capillary vessels are recognized as neoplastic; weak, or invisible VPI, and such meshed capillary vessels are considered nonneoplastic^[14-15].

Kudo's pit pattern types III–V are recognized as neoplastic, and Kudo's pit pattern types I–II are considered nonneoplastic when magnifying chromoendoscopy is used for observation. Moreover, the classification of pit patterns proposed by Kudo et al. can aid in accurate differentiation between neoplastic from nonneoplastic lesions when magnifying NBI is used^[16]. Several studies have combined magnifying colonoscopy or HRE and chromoendoscopy or NBI to differentiate between hyperplastic and neoplastic polyps. With these combinations, higher accuracy can be achieved when compared with conventional white-light endoscopy^[4,16]. However, HRE and magnifying colonoscopy are still not widely used and thus cannot replace conventional colonoscopy in routine clinical practice in Taiwan. Therefore, conventional colonoscopy cannot adequately achieve accurate differentiation between various types of colon polyps. Our study aimed to evaluate the diagnostic performance of computer-aided methods in distinguishing colorectal polyps using conventional colonoscopy with and without NBI, and possible causes of differences in diagnostic performance for both types of lesions.

Descriptive statistics quantitatively describe characteristics of a collection of numerical data. Mean and median values are commonly utilized to measure the central tendency of data. The standard deviation, which summarizes the difference of each data point from the mean, depicts the variability of the data set. Compared with the normal distribution, the shape of the data set can be described by skew and kurtosis. Furthermore, the probability of occurrence for each data point was integrated to measure the entropy and energy. Entropy and energy are widely used to determine the uncertainty or the complexity of a system, which is comparable to the situation when we attempt to diagnose an uncertain polyp, detected using white-light or NBI images.

Both light sources used in the video endoscope imaging system were respectively utilized to examine the colorectal polyp. One light source (white light)

used standard optical filters, and the other used narrow-band filters. For any of the light sources, received intensities in every filter band were synthesized and sequentially generated colored endoscopic images. The digital color image used three components, including red, green, and blue colors, to represent the color space for display on the monitor. Received intensities in each filter were thereby stored in one of the image components.

The spectral information of a polyp in each component of its color image describes characteristics reflected from the corresponding filter band. Using gradient operations, the abruptness at a pixel could be quantitatively measured. Pixels with a higher gradient magnitude indicate an abrupt interface at these positions in the image. Therefore, gradient magnitudes derived from this spectral information are utilized to measure the heterogeneousness of a polyp. In this study, both spectral information and gradient magnitudes were objectively characterized using the mean, median, standard deviation (SD), skew, kurtosis, entropy, and energy. Diagnostic values of each individual feature in differentiating neoplastic from nonneoplastic lesions were evaluated. Further, a computer-aided diagnosis system, which provided auxiliary information in the clinical diagnosis, was constructed to predict histopathologies of all polyps.

Methods

Patients

This study enrolled 36 colorectal polyps from consecutive patients who underwent colonoscopy at Tungs' Taichung MetroHarbor Hospital between November and December 2010. All polyps were polypectomized or biopsied for histological diagnosis after observation during the colonoscopy.

Endoscopy and NBI system

A standard videoendoscopy system (EVIS LUCERA 260 system, Olympus Optical, Tokyo, Japan) incorporated with NBI function was used for this study. NBI utilizes two narrow-band illuminations of 415 and 540 nm, with bandwidths of 30 nm and 20 nm, respectively. Conventional colonoscopes (CF240, CF260, and CF260L) were used for examination.

Image evaluation

When a polyp was encountered, the lesion was

first observed using white light. Thereafter, the light source was shifted to the NBI system with a control knob on the grip of the endoscope, and the same lesion was reevaluated. All endoscopic images that were photographed under both WL and NBI were stored in a digital image filing system as JPEG files.

For any lesion, we selected one image with the best quality and a distinguishable border from normal colon mucosa for analysis. The image of the polyp part was totally enclosed manually along a distinguishable border (Fig 2). The brightest part induced by the endoscopic light reflection within the enclosed image was excluded. Further, the residual part of the image was left for the analysis. Spectral information from red, green, and blue components of each image, including mean, median, SD, skew, kurt, entropy, and energy, were recorded.

Computerized polyp features

The central tendency, dispersion, and shape for a set of intensities were described using descriptive statistics. The arithmetic average of intensities was measured by the following formula:

$$Mean = \frac{\sum_{(x,y) \text{ in Lesion}} I(x,y)}{S(Lesion)} \tag{1}$$

where $I(x, y)$ indicates the intensity in pixels (x, y) and $S(Lesion)$ represents the lesion size. The *median* is the middle value of intensities in their numerical order. The standard deviation (*SD*) of intensities was measured by the following formula:

$$SD = \sqrt{\frac{\sum_{(x,y) \text{ in Lesion}} (I(x,y) - mean)^2}{S(Lesion) - 1}} \tag{2}$$

The skew of intensities was evaluated by the following formula:

$$Skew = \frac{S(Lesion)}{(S(Lesion) - 1)(S(Lesion) - 2)} \sum_{(x,y) \text{ in Lesion}} \left(\frac{I(x,y) - mean}{SD} \right)^3 \tag{3}$$

The kurtosis of intensities was measured by:

$$Kurt = \left\{ \frac{S(Lesion) * (S(Lesion) + 1)}{(S(Lesion) - 1)(S(Lesion) - 2)(S(Lesion) - 3)} \sum_{(x,y) \text{ in Lesion}} \left(\frac{I(x,y) - mean}{SD} \right)^4 \right\} - \frac{3((S(Lesion) - 1)^2)}{(S(Lesion) - 2)(S(Lesion) - 3)} \tag{4}$$

The probability of occurrence for an intensity value was defined as follows:

$$P(I) = \frac{S(I)}{S(Lesion)} \tag{5}$$

where $S(I)$ represents the total number of pixels with intensity I . Entropy and energy features were defined as follows:

$$Energy = \sum_{I \in \text{All intensities}} P(I)^2 \tag{6}$$

$$Entropy = \sum_{I \in \text{All intensities}} P(I) \log P(I) \tag{7}$$

Finally, *mean, median, SD, skew, kurt, entropy, and energy* features were defined as computerized polyp features.

In colored endoscopic images, intensities stored in a component described characteristics reflected from the corresponding filter band. For each component, intensities in the identified polyp were described on the basis of computerized polyp features. Furthermore, the gradient at a pixel contained derivate approximations in horizontal and vertical directions, as follows:

$$G_x = [I(x + 1, y - 1) + 2I(x + 1, y) + I(x + 1, y + 1)] - [I(x - 1, y - 1) + 2I(x - 1, y) + I(x - 1, y + 1)] \tag{8}$$

$$G_y = [I(x - 1, y - 1) + 2I(x, y - 1) + I(x + 1, y - 1)] - [I(x - 1, y + 1) + 2I(x, y + 1) + I(x + 1, y + 1)] \tag{9}$$

The gradient magnitude at a pixel was evaluated as follows:

$$G_{(x,y)} = \sqrt{G_x^2 + G_y^2} \tag{10}$$

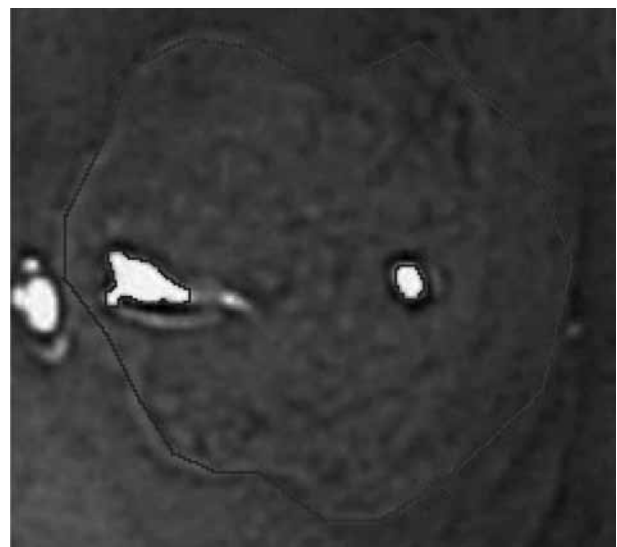


Fig. 2 Image of polyp part was totally enclosed manually along distinguishable border . The most bright part induced by endoscopic light reflection within the enclosed image was quit

Each component of the colorectal image was transformed to gradient images using above formulas. Moreover, gradient magnitudes in the area of the identified polyp were described on the basis of computerized polyp features.

Statistical methods

The ability of each computerized polyp feature to differentiate nonneoplastic lesions from neoplastic lesions was measured using Student's t-test. Before the test, the Levene's test was performed to verify the equality of variance between both groups. In both tests, the significance level was defined as 0.05. The differentiating ability was further measured using a receiver operating characteristic (ROC) curve for features with significant differences in the t-test. The correlation between computerized polyp features and pathology results was formulated using the binary logistic regression model. Although all computerized features were employed in the regression, an over-fitting problem led to the failure of the constructed model. The forward feature selection was utilized to evaluate the contribution of each computerized feature for the regression model. Features with significant contributions were adopted to construct the regression model as a computer-aided diagnosis (CAD) system. This computer-aided diagnosis system was further verified by using the leave-one-out method. During verification, each case

was diagnosed by the CAD system constructed using remaining cases. Finally, all results were integrated to evaluate the diagnostic performance of the CAD system.

Results

Thirty-six polyps were enrolled in this study. Both WL and NBI images were available for 29 polyps, NBI images alone were available for six polyps, and a WL image alone was available for one polyp. Thirty WL images were analyzed: 15 adenomatous polyps and 15 hyperplasia polyps. Thirty-five NBI images were analyzed: 18 adenomatous polyps and 17 hyperplasia polyps.

Differentiating the ability of computerized spectral characteristics

To comprehensively explore the efficacy of the spectral and gradient image information in differentiating the histopathology of colorectal lesions, we generated characterized features from the tumor's intensities using red, green, and blue components. Thereafter, we evaluated their diagnostic values for distinguishing adenomatous polyps from hyperplastic polyps, as presented in Tables 2 and 3 and Figure 3.

For red, green, and blue components of white-light images, statistically significant differences were observed between hyperplastic and adenomatous

Table 2. The spectral information in the determined polyp was described by the computerized features. The difference between hyperplasia and adenomas on each computerized feature was measured by the t-test.

Image Type	Component	Feature	Pathology	Mean±SD	Levene's Test	t-test		
						Sig.	95% CI	
							Lower	Upper
White Light	Red	<i>Mean</i>	Hyperplasia	163.44±18.36	0.21	0.10	-27.89	2.75
			Adenomas	176.01±22.41				
		<i>Median</i>	Hyperplasia	164.93±19.43	0.21	0.09	-30.22	2.49
			Adenomas	178.80±24.05				
		<i>SD</i>	Hyperplasia	10.23±3.57	0.01	0.04	-10.23	-0.22
			Adenomas	15.46±8.53				
		<i>Skew</i>	Hyperplasia	-0.74±0.76	0.00	0.58	-0.58	0.33
			Adenomas	-0.61±0.37				
		<i>Kurt</i>	Hyperplasia	3.92±4.28	0.00	0.01	1.17	5.94
			Adenomas	0.36±0.63				
		<i>Entropy</i>	Hyperplasia	5.15±0.43	0.13	0.01	-0.93	-0.14
			Adenomas	5.68±0.61				

Table 2. Countinued

Image Type	Component	Feature	Pathology	Mean±SD	Levene's Test	t-test		
						Sig.	95% CI	
							Lower	Upper
White Light	Red	<i>Energy</i>	Hyperplasia	36.15±11.38	0.42	0.01	3.46	19.29
			Adenomas	24.78±9.72				
	<i>Mean</i>	Hyperplasia	106.10±16.34	0.77	0.76	-10.68	14.43	
		Adenomas	104.22±17.23					
	<i>Median</i>	Hyperplasia	107.40±17.97	0.97	0.84	-12.15	14.82	
		Adenomas	106.07±18.08					
	<i>SD</i>	Hyperplasia	13.36±5.13	0.06	0.01	-12.23	-2.10	
		Adenomas	20.53±8.09					
	Green	<i>Skew</i>	Hyperplasia	-0.23±0.81	0.03	0.69	-0.38	0.57
			Adenomas	-0.33±0.35				
	<i>Kurt</i>	Hyperplasia	2.56±3.45	0.00	0.01	0.80	4.67	
		Adenomas	-0.18±0.67					
	<i>Entropy</i>	Hyperplasia	5.54±0.48	0.35	0.00	-1.05	-0.29	
		Adenomas	6.21±0.54					
	<i>Energy</i>	Hyperplasia	27.52±8.74	0.18	0.00	5.42	16.54	
		Adenomas	16.54±5.84					
	<i>Mean</i>	Hyperplasia	77.53±15.88	0.82	0.87	-12.67	10.75	
		Adenomas	78.50±15.44					
	<i>Median</i>	Hyperplasia	78.67±17.02	0.84	0.89	-13.42	11.69	
		Adenomas	79.53±16.55					
	<i>SD</i>	Hyperplasia	12.72±5.02	0.26	0.03	-8.92	-0.60	
		Adenomas	17.48±6.05					
	Blue	<i>Skew</i>	Hyperplasia	-0.12±0.82	0.02	0.84	-0.43	0.53
			Adenomas	-0.17±0.35				
<i>Kurt</i>	Hyperplasia	3.29±4.22	0.00	0.01	0.93	5.67		
	Adenomas	-0.01±0.84						
<i>Entropy</i>	Hyperplasia	5.47±0.49	0.94	0.00	-0.90	-0.19		
	Adenomas	6.02±0.46						
<i>Energy</i>	Hyperplasia	28.77±9.36	0.10	0.00	4.65	16.13		
	Adenomas	18.38±5.49						
<i>Mean</i>	Hyperplasia	114.10±20.53	0.15	0.99	-18.09	18.35		
	Adenomas	113.97±31.05						
<i>Median</i>	Hyperplasia	115.65±21.23	0.15	0.95	-18.42	19.71		
	Adenomas	115.00±32.64						
NBI	Red	SD	Hyperplasia	17.20±6.67	0.50	0.07	-9.45	0.30
			Adenomas	21.77±7.44				
	Skew	Hyperplasia	-0.37±0.53	0.98	0.44	-0.50	0.22	
		Adenomas	-0.23±0.53					
	Kurt	Hyperplasia	1.03±2.08	0.04	0.30	-0.60	1.86	
		Adenomas	0.40±1.39					

Table 2. Countinued

Image Type	Component	Feature	Pathology	Mean±SD	Levene's Test	t-test			
						Sig.	95% CI		
							Lower	Upper	
NBI	Red	Entropy	Hyperplasia	5.95±0.53	0.93	0.04	-0.75	-0.02	
			Adenomas	6.33±0.52					
		Energy	Hyperplasia	20.51±7.91	0.17	0.05	0.12	9.87	
			Adenomas	15.51±6.21					
		Mean	Hyperplasia	69.72±16.66	0.45	0.05	-24.72	-0.17	
			Adenomas	82.17±18.88					
	Median	Hyperplasia	69.65±17.90	0.40	0.07	-26.46	0.86		
		Adenomas	82.44±21.53						
	SD	Hyperplasia	17.29±6.16	0.55	0.01	-10.47	-1.58		
		Adenomas	23.32±6.72						
	Green	Skew	Hyperplasia	0.20±0.73	0.39	0.56	-0.31	0.56	
			Adenomas	0.07±0.53					
		Kurt	Hyperplasia	1.64±2.73	0.00	0.04	0.10	3.00	
			Adenomas	0.09±0.89					
		Blue	Entropy	Hyperplasia	5.95±0.47	0.65	0.00	-0.81	-0.20
				Adenomas	6.45±0.42				
	Energy		Hyperplasia	20.08±7.41	0.06	0.01	2.05	10.37	
			Adenomas	13.87±4.38					
	Mean		Hyperplasia	55.93±13.36	0.46	0.16	-17.64	3.08	
			Adenomas	63.21±16.50					
	Median	Hyperplasia	55.53±14.31	0.40	0.21	-18.85	4.24		
		Adenomas	62.83±18.81						
	SD	Hyperplasia	14.33±5.16	0.53	0.01	-8.90	-1.59		
		Adenomas	19.57±5.45						
Blue	Skew	Hyperplasia	0.35±0.82	0.31	0.51	-0.33	0.65		
		Adenomas	0.19±0.57						
	Kurt	Hyperplasia	2.50±3.83	0.00	0.04	0.09	4.16		
		Adenomas	0.37±1.22						
	Entropy	Hyperplasia	5.67±0.46	0.47	0.00	-0.82	-0.23		
		Adenomas	6.20±0.40						
Energy	Hyperplasia	24.40±8.47	0.04	0.00	3.00	12.75			
	Adenomas	16.52±5.04							

polyps for some characteristics such as SD, kurt, entropy, and energy. Further, the distribution of two pathologies in the same evaluation method was similar, even among different color components. Adenomatous polyps scored higher evaluations than hyperplastic ones with regard to SD and entropy characteristics. The spectral distribution of hyperplastic

polyps was generally more leptokurtic. Moreover, evaluations for energy in hyperplastic polyps were larger compared with those for adenomas.

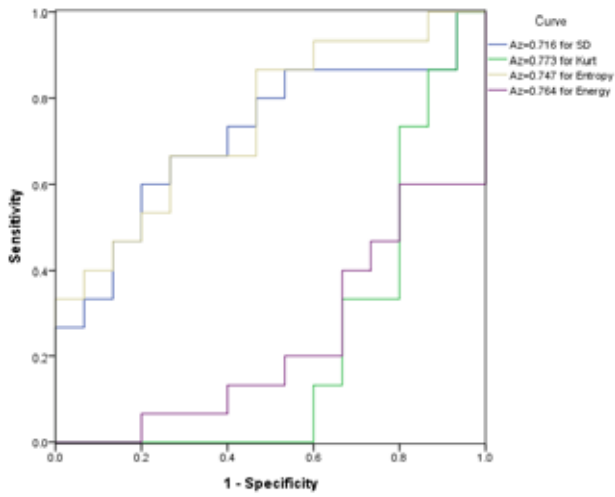
Furthermore, significance of differences between hyperplastic and adenomatous polyps of proposed spectral characteristics for red, green, and blue components of NBI were measured. Differences in entropy

Table 3. The gradient magnitude in the determined polyp was described by the computerized features. The difference between hyperplasia and adenomas on each computerized feature was measured by the t-test.

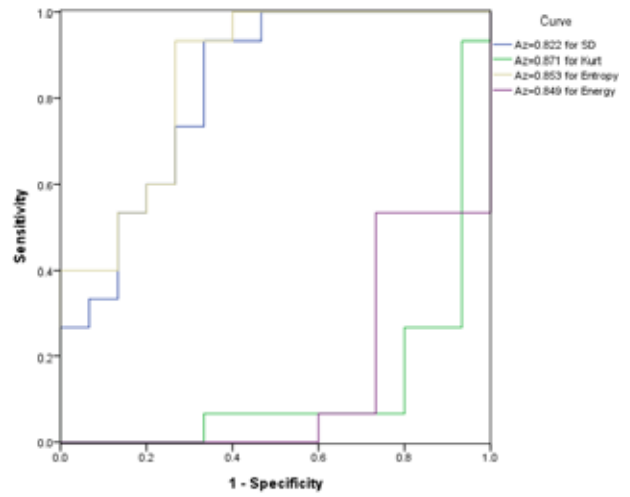
Image Type	Component	Feature	Pathology	Mean±SD	Levene's Test	t-test		
						Sig.	95% CI	
							Lower	Upper
WL	Red	<i>Mean</i>	Hyperplasia	19.50±4.37	0.17	0.02	-8.77	-0.70
			Adenomas	24.24±6.26				
		<i>Median</i>	Hyperplasia	15.45±3.60	0.12	0.01	-8.11	-1.39
			Adenomas	20.20±5.24				
		<i>SD</i>	Hyperplasia	17.97±6.50	0.16	0.91	-4.01	4.46
			Adenomas	17.75±4.68				
		<i>Skew</i>	Hyperplasia	3.83±1.77	0.01	0.01	0.55	2.61
			Adenomas	2.25±0.69				
		<i>Kurt</i>	Hyperplasia	27.21±22.25	0.01	0.01	4.98	30.13
			Adenomas	9.66±5.62				
		<i>Entropy</i>	Hyperplasia	5.38±0.34	0.55	0.02	-0.64	-0.07
			Adenomas	5.74±0.41				
	<i>Energy</i>	Hyperplasia	32.49±7.38	1.00	0.01	2.26	13.28	
		Adenomas	24.72±7.35					
	Green	<i>Mean</i>	Hyperplasia	21.28±5.09	0.07	0.01	-12.64	-1.95
			Adenomas	28.57±8.73				
		<i>Median</i>	Hyperplasia	16.63±4.15	0.05	0.00	-11.40	-2.66
			Adenomas	23.67±7.04				
		<i>SD</i>	Hyperplasia	20.60±7.72	0.42	0.81	-5.99	4.72
			Adenomas	21.24±6.55				
		<i>Skew</i>	Hyperplasia	4.16±1.99	0.08	0.00	0.64	3.00
			Adenomas	2.34±1.01				
		<i>Kurt</i>	Hyperplasia	32.57±29.51	0.10	0.01	4.58	37.96
			Adenomas	11.29±11.19				
<i>Entropy</i>		Hyperplasia	5.51±0.35	0.36	0.01	-0.78	-0.14	
		Adenomas	5.97±0.49					
<i>Energy</i>	Hyperplasia	30.06±7.20	0.84	0.00	3.19	14.25		
	Adenomas	21.34±7.59						
<i>Mean</i>	Hyperplasia	21.59±5.07	0.29	0.02	-10.44	-1.11		
	Adenomas	27.37±7.22						
<i>Median</i>	Hyperplasia	16.89±3.86	0.09	0.00	-9.78	-2.19		
	Adenomas	22.88±6.04						
<i>SD</i>	Hyperplasia	21.10±8.21	0.03	0.68	-4.10	6.15		
	Adenomas	20.07±4.98						
Blue	<i>Skew</i>	Hyperplasia	4.20±2.11	0.10	0.01	0.48	2.94	
		Adenomas	2.49±0.96					
	<i>Kurt</i>	Hyperplasia	33.36±34.02	0.17	0.05	0.45	38.55	
		Adenomas	13.87±11.83					
	<i>Entropy</i>	Hyperplasia	5.53±0.35	0.75	0.01	-0.68	-0.10	
		Adenomas	5.91±0.43					
<i>Energy</i>	Hyperplasia	29.54±6.92	0.90	0.01	2.53	12.88		
Adenomas	21.84±6.91							

Table 3. Countinued

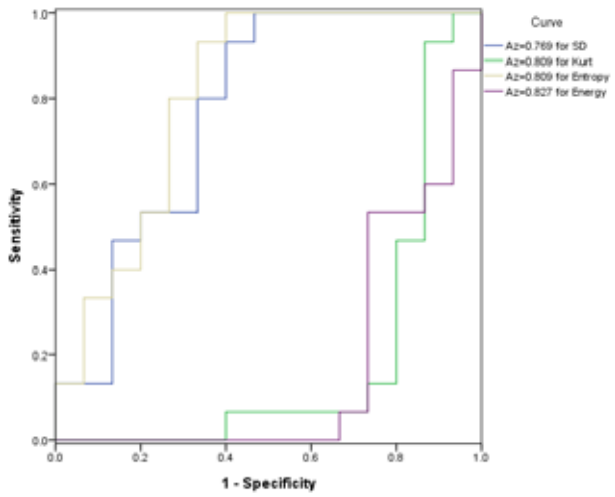
Image Type	Component	Feature	Pathology	Mean±SD	Levene's Test	t-test		
						Sig.	95% CI	
							Lower	Upper
NBI	Red	<i>Mean</i>	Hyperplasia	20.92±5.15	0.01	0.00	-20.14	-8.42
			Adenomas	35.20±10.84				
		<i>Median</i>	Hyperplasia	16.65±3.11	0.00	0.00	-16.67	-7.61
			Adenomas	28.79±8.68				
		<i>SD</i>	Hyperplasia	19.48±9.29	0.89	0.03	-13.62	-0.81
			Adenomas	26.70±9.33				
		<i>Skew</i>	Hyperplasia	3.93±2.08	0.01	0.01	0.57	2.85
			Adenomas	2.22±0.91				
		<i>Kurt</i>	Hyperplasia	31.28±27.79	0.00	0.01	6.44	36.03
			Adenomas	10.05±9.10				
		<i>Entropy</i>	Hyperplasia	5.49±0.36	0.15	0.00	-1.10	-0.48
			Adenomas	6.28±0.52				
	<i>Energy</i>	Hyperplasia	29.47±5.91	0.68	0.00	7.58	16.60	
		Adenomas	17.37±7.10					
	Green	<i>Mean</i>	Hyperplasia	21.70±5.70	0.01	0.00	-22.49	-9.78
			Adenomas	37.84±11.71				
		<i>Median</i>	Hyperplasia	16.65±3.40	0.00	0.00	-18.92	-9.11
			Adenomas	30.66±9.39				
		<i>SD</i>	Hyperplasia	22.48±10.46	0.94	0.07	-13.63	0.50
			Adenomas	29.05±10.08				
		<i>Skew</i>	Hyperplasia	4.64±2.06	0.01	0.00	1.43	3.66
			Adenomas	2.10±0.83				
		<i>Kurt</i>	Hyperplasia	40.29±26.76	0.00	0.00	17.62	45.88
			Adenomas	8.54±7.69				
<i>Entropy</i>		Hyperplasia	5.55±0.37	0.16	0.00	-1.17	-0.55	
		Adenomas	6.41±0.52					
<i>Energy</i>	Hyperplasia	28.92±6.00	0.98	0.00	8.62	17.25		
	Adenomas	15.98±6.52						
<i>Mean</i>	Hyperplasia	20.92±5.34	0.00	0.00	-21.06	-9.08		
	Adenomas	35.99±11.04						
<i>Median</i>	Hyperplasia	16.07±3.07	0.00	0.00	-17.60	-8.44		
	Adenomas	29.09±8.81						
Blue	<i>SD</i>	Hyperplasia	21.67±10.13	0.99	0.07	-12.99	0.64	
		Adenomas	27.85±9.68					
<i>Skew</i>	Hyperplasia	4.75±2.02	0.01	0.00	1.50	3.70		
	Adenomas	2.15±0.86						
<i>Kurt</i>	Hyperplasia	41.94±26.15	0.00	0.00	18.93	46.68		
	Adenomas	9.14±8.18						
<i>Entropy</i>	Hyperplasia	5.49±0.35	0.16	0.00	-1.15	-0.54		
	Adenomas	6.34±0.52						
Blue	<i>Energy</i>	Hyperplasia	30.10±5.98	0.91	0.00	8.84	17.71	
		Adenomas	16.82±6.86					



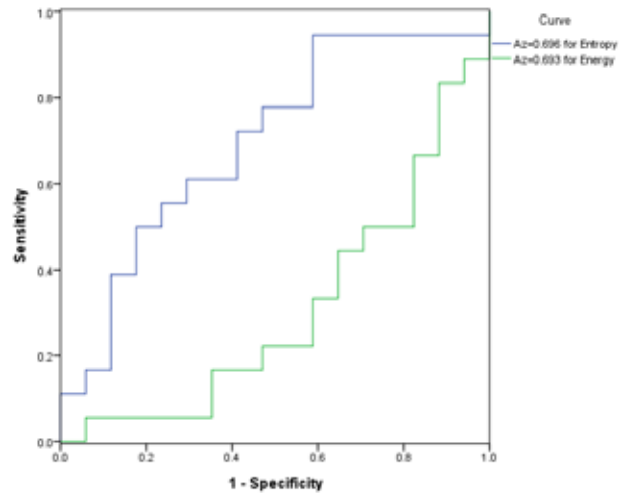
(a) Red component in WL image



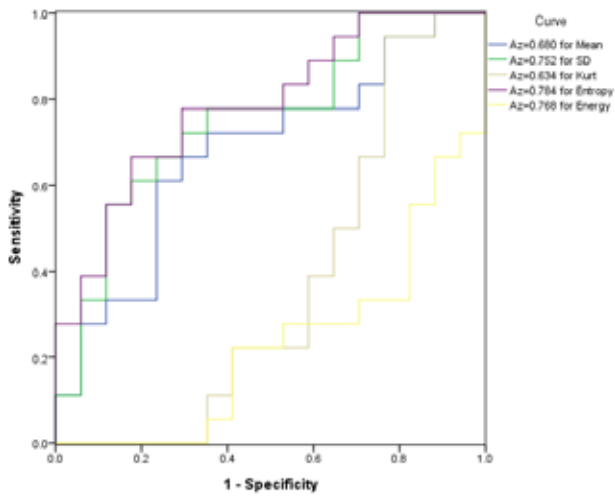
(b) Green component in WL image



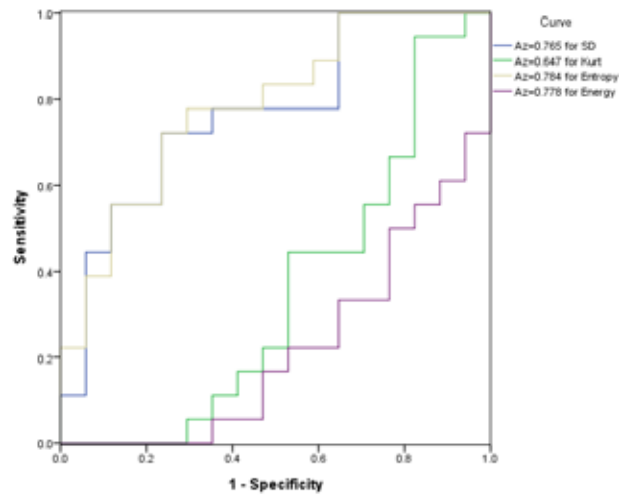
(c) Blue component in WL image



(d) Red component in NBI image



(e) Green component in NBI image



(f) Blue component in WL image

Fig. 3 The ability for differentiating adenomas from hyperplasia on computerized polyp features was evaluated by ROC analysis.

and energy characteristics were statistically significant in each component. For green and blue components, differences between SD and Kurt characteristics were statistically significant. The mean of adenomatous polyps was significantly larger compared with the mean of the hyperplastic polyp in the green component. The distribution of two pathologies for few characteristics such as entropy, energy, SD, and kurt in NBI were equivalent to that in white-light images.

For red, green, and blue components of both white-light and narrow-band images, statistically significant differences were observed between hyperplastic and adenomas polyps with regard to characteristics of the gradient magnitude, including mean, median, skew, kurt, entropy, and energy. In addition, the difference in the gradient magnitude was significant for the red component of NBI. The distribution of both pathologies in the same evaluation method was similar, even among different color components. Adenomatous polyps scored higher gradient magnitudes compared with hyperplastic polyps with regard to mean, median, and entropy characteristics. Moreover, gradient magnitudes of hyperplastic polyps were generally more leptokurtic. Furthermore, gradient magnitudes of skew and energy for hyperplastic polyps were higher compared with those for adenomas.

The differentiating ability between two colorectal histopathologies for spectral characteristics, which were significant in previous examinations, was further evaluated by ROC analysis. For white-light images, Az values for characteristics, including SD, kurt, entropy, and energy, in the green component

were obviously higher compared with those for other components. SD, entropy, and energy characteristics in green and blue components of NBI demonstrated more differentiating abilities compared with those in the red components.

To avoid the over-fitting problem, the forward feature selection method was adopted to evaluate the contribution of each computerized polyp feature in the construction of the CAD system. Two features, including the kurtosis of intensities in the green component and the median of gradient magnitudes in the green component, were adopted to construct the CAD system for white-light images. The energy of gradient magnitudes in the green component and the skew of gradient magnitudes in the blue component were utilized to construct the CAD system for narrow-band images.

To verify the diagnostic performance of the constructed CAD system, the leave-one-out method was adopted. The probability of each adenoma was calculated using the CAD system constructed by remaining cases in the same image type. Corresponding probabilities for all adenomas were available. All probabilities were finally integrated to evaluate the diagnostic performance using ROC analysis, as presented in Figure 4. The area under the curve was 0.827 and 0.951 for CAD systems using white-light images and those using narrow-band images, respectively. Histograms demonstrated distributions of predicted probabilities of hyperplasia and adenomas for both CAD systems in Figure 5. Although the cut-off value was set at 0.6, diagnostic performances for both CAD systems have been listed

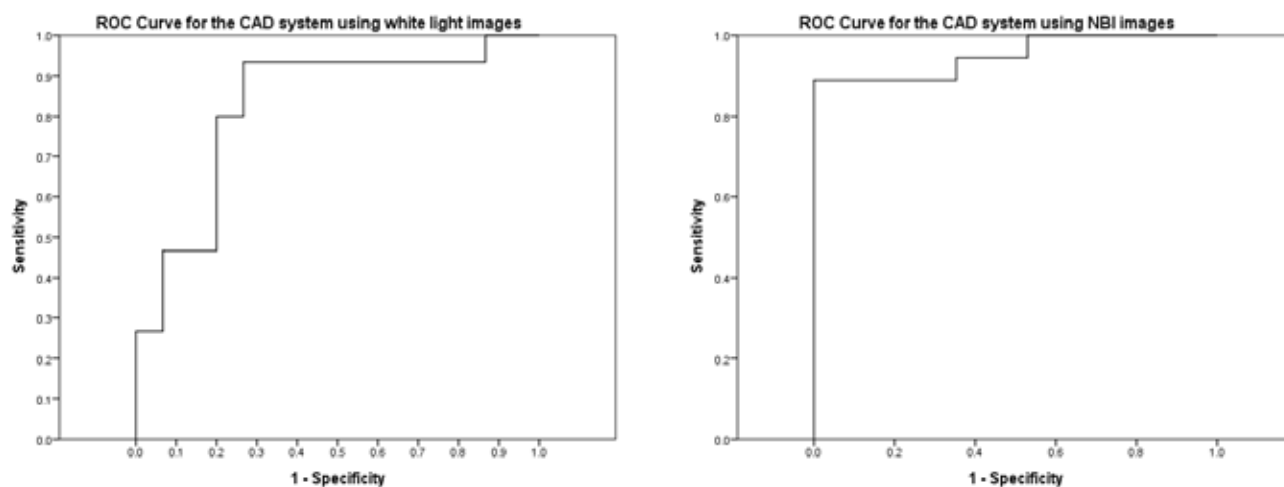


Fig. 4 The ROC curves for the CAD systems using WL images (left)and using NBI images (right).

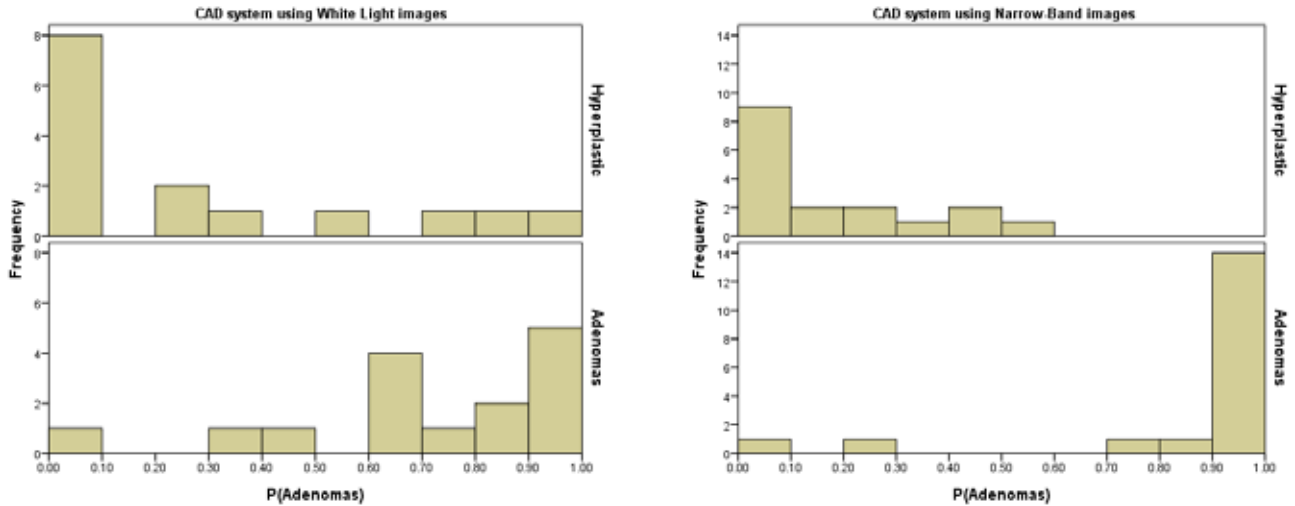


Fig. 5 The probability for predicting a polyp as adenomas was measured by the CAD system. The histograms show the distribution of all probabilities predicted by the CAD system using WL images or using NBI images. Further, the histograms in the same image type were separately represented in the different lesion types.

Table 4. The diagnostic performance of CAD system using white light images.

Pathology	CAD system		Accuracy
	Hyperplasia	Adenomas	
Hyperplasia	12	3	80%
Adenomas	3	12	80%
Accuracy	80%	80%	80%

Table 5. The diagnostic performance of CAD system using narrow band images.

Pathology	CAD system		Accuracy
	Hyperplasia	Adenomas	
Hyperplasia	17	0	100%
Adenomas	2	16	88.9%
Accuracy	89.8%	100%	94.2%

in Tables 4 and 5. Performance indices for accuracy, sensitivity, specificity, positive predictive value, and negative predictive value were all 80% for the CAD system using white-light images. In addition, performance indices for accuracy, sensitivity, specificity, positive predict value, and negative predictive value were 94.2%, 88.9%, 100%, 100%, and 89.8%, respectively, for the CAD system using narrow-band images.

Discussion

It is essential to differentiate neoplastic lesions from nonneoplastic lesions because most colorectal cancers arise from previously benign adenomas through the adenoma–carcinoma sequence^[1]. Accordingly, we could limit and avoid risks associated with polypectomy, including perforation and bleeding, if a more accurate method of differentiation was available. The classification of the mucosal pit pattern of colorectal neoplasia has been established since its introduction in 1994 by Kudo et al.^[17]; an

accuracy as high as 90% was achieved with this classification of the pit pattern (type I and II are nonneoplastic, whereas type III, IV, and V are neoplastic)^[18]. Moreover, significantly higher accuracy has been achieved under NBI with magnification compared with conventional white-light endoscopy^[4,16]. Further, NBI without magnification provided significant accuracy and sensitivity compared with conventional white-light endoscopy^[4,6].

Kudo et al. proposed the pit pattern of differentiating colonic polyps via magnifying chromoendoscopy^[9]. Type I pit pattern: normal round pit; type II: stellar or papillary pits; type III: small tubular or round pits; type III-L: large tubular pits; type IV: sulcus or gyrus pits; and type V: nonstructural pits. Average pits size were 0.07 mm, 0.09 mm, 0.03 mm, 0.22 mm, and 0.93 mm for type I to IV pit patterns, respectively^[19]. Type II pit pattern has been recognized as hyperplastic polyps, and type IIIs, III-L, and IV correspond to adenomas.

No statistically significant difference was

observed between an adenoma and a hyperplastic polyp in mean and median characteristics of red, green, and blue components of WL images. For red, green, and blue components of WL images, statistically significant differences were observed between hyperplastic polyps and adenomatous polyps for *SD*, *Kurt*, *Entropy*, and *Energy* characteristics. The distribution of both pathologies in the same evaluation method was similar, even in different color components. The information provided by lower *SD* and entropy scores correspond to leptokurtic characteristics and higher scores for energy in hyperplastic polyps. Apparently, spectra in adenomas were more widely distributed compared with spectra in hyperplasia polyps. The pit size in types III and IV lesions was larger compared with that in type II lesions. Without magnifying chromoendoscopy, type II pits could not be detected. Type III and IV pit patterns were detected in few adenomas with WL without magnification; under low magnification, this rendered hyperplastic surfaces more homogeneous when compared with adenomatous polyps. In addition, this explained the information from the computer-analyzed spectral distribution of WL images in our study.

The significance of differences between hyperplastic polyps and adenomas for *SD* and *kurt* characteristics in the red component under NBI was lost when compared with that using WL, but the significance of differences between energy and entropy characteristics were retained. The actual narrow-band green light (540 nm, bandwidth 20 nm) was reassigned to the red component during the NBI observation. The absorption capability of green light by oxyhemoglobin was less compared with that of the blue light. Besides, the band width was restricted to 20 nm before the redistribution and reassignment of the green light. These factors may contribute to the lost significance of differences between *SD* and *kurt* characteristics.

For green and blue components in NBI, statistically significant differences of *SD*, *kurt*, *entropy*, and *energy* characteristics corresponded to their counterparts in WL. Notably, the mean of green components under NBI revealed significant differences between both lesions. Under NBI, the actual narrow-band blue light (415 nm, band width 30 nm) was reassigned to green and blue components, respectively. The average mean score of the green component under

NBI was 69.72 for hyperplastic polyps and 82.17 for adenomas. The vascular portion within the adenoma heavily absorbed the NBI blue light. However, the NBI blue light penetration was more superficial compared with that of the green and red light. Deep penetration of the NBI blue light into the nonvascular portion within the adenoma was prevented by convoluted and deeper pit pattern growth. Because of the difference in the absorption capability between vascular and nonvascular portions within an adenomatous polyp, significant differences were observed between both lesion types under NBI green components.

We used different features in WL and NBI to construct the CAD system. Two features of the green component were adopted to construct the CAD system for WL and one feature each of the green and the blue component were used for NBI. Red component features were not helpful in constructing the CAD system because red light was more poorly absorbed by lesions compared with other colors. By analyzing this spectral information, we determined that the accuracy of the computer-aided diagnostic performance was higher by NBI than by WL; moreover, these findings were compatible with previous findings from clinical studies without computer-aided analysis.

In summary, the difference between neoplastic and nonneoplastic lesions was significant for several features of spectral information and gradient magnitudes. Green and blue components played a more important role than the red component not only in NBI but also in WL in discriminating between both types of lesions. The accuracy of the computer-aided diagnostic performance with the use of spectral information was higher in NBI than in WL.

Reference

1. Vogelstein B, Fearon ER, Hamilton SR, Kern SE, Preisinger AC, Leppert M, Nakamura Y, White R, Smits AM, Bos JL. Genetic alterations during colorectal-tumor development. *N Engl J Med*. 1988 Sep 1;319(9):525-32.
2. Winawer SJ, Zauber AG, Ho MN, O'Brien MJ, Gottlieb LS, Sternberg SS, Waye JD, Schapiro M, Bond JH, Panish JF, et al. Prevention of colorectal cancer by colonoscopic polypectomy. The National Polyp Study Workgroup. *N Engl J Med*. 1993 Dec 30;329(27):1977-81.
3. East JE, Saunders BP, Jass JR. Sporadic and syndromic hyperplasia polyps and serrated adenomas of the colon: classification, molecular genetics, natural history, and clinical management. *Gastroenterol Clin North Am*. 2008 Mar; 37(1):25-46, v. Review.

4. Chiu HM, Chang CY, Chen CC, Lee YC, Wu MS, Lin JT, Shun CT, Wang HP. A prospective comparative study of narrow-band imaging, chromoendoscopy, and conventional colonoscopy in the diagnosis of colorectal neoplasia. *Gut*. 2007 Mar;56(3):373-9.
5. Bruno MJ. Magnification endoscopy, high resolution endoscopy, and chromoscopy; towards a better optical diagnosis. *Gut*. 2003 Jun;52Suppl 4:iv7-11. Review.
6. Su MY, Hsu CM, Ho YP, Chen PC, Lin CJ, Chiu CT. Comparative study of conventional colonoscopy, chromoendoscopy, and narrow-band imaging systems in differential diagnosis of neoplastic and nonneoplastic colonic polyps. *Am J Gastroenterol*. 2006 Dec;101(12):2711-6.
7. Fujii T, Hasegawa RT, Saitoh Y, Fleischer D, Saito Y, Sano Y, Kato S. Chromoscopy during colonoscopy. *Endoscopy*. 2001 Dec;33(12):1036-41. Review.
8. Hurlstone DP, Fujii T. Practical uses of chromoendoscopy and magnification at colonoscopy. *GastrointestEndoscClin N Am*. 2005 Oct;15(4):687-702. Review.
9. Kudo S, Tamura S, Nakajima T, Yamano H, Kusaka H, Watanabe H. Diagnosis of colorectal tumorous lesions by magnifying endoscopy. *GastrointestEndosc*. 1996 Jul;44(1):8-14.
10. Gono K, Obi T, Yamaguchi M, Ohyama N, Machida H, Sano Y, Yoshida S, Hamamoto, Endo T. Appearance of enhanced tissue features in narrow-band endoscopic imaging. *J Biomed Opt*. 2004 May-Jun;9(3):568-77.
11. Yoshida T, Inoue H, Usui S, Satodate H, Fukami N, Kudo SE. Narrow-band imaging system with magnifying endoscopy for superficial esophageal lesions. *GastrointestEndosc*. 2004 Feb;59(2):288-95.
12. Muto M, Katada C, Sano Y, Yoshida S. Narrow band imaging: a new diagnostic approach to visualize angiogenesis in superficial neoplasia. *ClinGastroenterolHepatol*. 2005 Jul;3(7 Suppl 1):S16-20. Review.
13. Kuznetsov K, Lambert R, Rey JF. Narrow-band imaging: potential and limitations. *Endoscopy*. 2006 Jan;38(1):76-81.
14. Sano Y, Horimatsu T, Fu KI, et al. Magnifying observation of micro-vascular architecture of colorectal lesions using narrow band imaging system. *Dig Endoscopy* 2006;18: S44-51.
15. East JE, Suzuki N, Bassett P, Stavrindis M, Thomas HJ, Guenther T, Tekkis PP, Saunders BP. Narrow band imaging with magnification for the characterization of small and diminutive colonic polyps: pit pattern and vascular pattern intensity. *Endoscopy*. 2008 Oct;40(10):811-7. Epub 2008 Sep 30.
16. Machida H, Sano Y, Hamamoto Y, et al. Narrow-band imaging in the diagnosis of colorectal mucosal lesions: a pilot study. *Endoscopy* 2004;36:1094-8.
17. Kudo S, Hirota S, Nakajima T, et al. Colorectal tumours and pit pattern. *J ClinPathol*1994;47:880-5.
18. Su MY, Ho YP, Chen PC, et al. Magnifying endoscopy with indigo carmine contrast for differential diagnosis of neoplastic and nonneoplastic colonic polyps. *Dig Dis Sci*2004;49:1123-7.
19. Paris Workshop Participants. The Paris endoscopic classification of superficial neoplastic lesions: esophagus., stomach and coon. *GastrointestEndosc* 2002;58:S3-43.
20. Rogart JN, Jain D, Siddiqui UD *et al*. Narrow-band imaging without high magnification to differentiate polyps during real-time colonoscopy: improvement with experience. *GastrointestEndosc*2008; 68: 1136-45 .

比較窄頻影像及傳統白光影像在區別大腸息肉之診斷表現

蔡明宏¹ 沈偉誌^{2*}

¹童綜合醫院 內科部胃腸肝膽科

²亞洲大學資訊工程學系

受文日期：民國 102 年 3 月 28 日；接受刊載：民國 102 年 11 月 27 日

摘要

大部分的大腸癌多經由良性的腺瘤演變而形成，因為有癌化的風險，腺瘤必須切除。如果我們能正確的分辨腺瘤與非腺瘤病灶，就可以避免非腺瘤的過度治療。

窄頻影像系統是新近發展的光學染色內視鏡，可以使得黏膜表淺的微細血管突顯，而沒有傳統染色內視鏡在觀察上需要人為噴灑染劑的不便。

為了提高診斷正確率，不論傳統染色內視鏡或窄頻影像系統，最好能搭配放大內視鏡，但是在臨床上，放大內視鏡的使用並不普遍。我們分析了 36 個息肉病灶在白光及窄頻影像下，其紅、綠、藍三種顏色的數位資料，除了窄頻影像紅光的 SD 及 Kurt 外，不論是否使用窄頻影像，兩者病灶在 SD、Kurt、Entropy 與 Energy 的特徵分析均呈現統計上的差異，可能是因為非腺瘤病灶呈現較均質黏膜表面。在窄頻影像中綠光的平均值在兩者病灶間亦呈明顯的差異，可能是腺瘤病灶具備較大的凹陷型態吸收較少的綠光而造成。在電腦輔助診斷的表現上，窄頻影像優於傳統白光，這與以往臨床上的研究結果相符。

關鍵詞：窄頻影像、白光、大腸息肉、電腦輔助診斷

Original Article

Apple Polyphenol Inhibits Lipopolysaccharide-induced Inflammation in an Animal Model

Huei-Jane Lee*

Institute of Biochemistry and Biotechnology, Chung Shan Medical University

Received: Dec. 22, 2013; Accepted: Jan. 8, 2014

ABSTRACT

Background and purpose: Previous studies demonstrate antioxidant effects of apple polyphenols (AP). In the present study, the potential anti-inflammatory effects of AP were examined in an animal model of lipopolysaccharide (LPS)-induced hepatic inflammation.

Methods: Rats were pretreated with AP for five days before intraperitoneal (i.p.) administration of 5 mg/kg LPS. After 6 h, the animals were sacrificed, and plasma alanine (ALT) levels, aspartate aminotransferase (AST) levels, glutathione (GSH) levels, catalase activity, and lipid peroxidation were assessed in liver tissues.

Results: Pretreatments with AP decreased hepatic LPS-induced ALT and AST levels. Moreover AP pretreatment preserved antioxidant catalase activity and glutathione (GSH) levels and decreased lipid peroxidation in the livers of LPS-treated rats. Histopathological evaluations of rat livers revealed that AP reduced the incidence of LPS-induced liver lesions and neutrophil infiltration.

Discussion: The present data indicate that AP has anti-inflammatory potential *in vivo* and could be developed as an anti-inflammatory agent.

Key words: Apple polyphenol, hepatotoxicity, anti-inflammatory

INTRODUCTION

Inflammation is a protective reaction to injury and infection and is characterized by heat, pain, and swelling. Acute inflammation is pivotal to the defense response, and chronic inflammation has been implicated in a wide variety of disorders, such as cardiovascular disease, cancer, diabetes, arthritis, Alzheimer's disease, pulmonary disease, and autoimmune diseases [1]. In addition, previous studies show that chronic inflammation is linked to various tumorigenic processes, including cellular transformation, promotion, survival, proliferation, invasion, angiogenesis, and metastasis of cancer cells [2].

In normal cells, cyclooxygenase-2 is expressed at extremely low levels, but is strongly induced by growth factors and pro-inflammatory molecules such as lipopolysaccharide (LPS) and is activated by several oncogene products [3]. Previous studies show that cyclooxygenase-2 inhibitors block prostaglandin E2 synthesis, thereby inhibiting inflammation and conferring analgesic effects [4]. Moreover, homozygous deletion of the cyclooxygenase-2 gene alleviates LPS-mediated hepatocellular toxicity [5]. Thus, it has been suggested that cyclooxygenase-2 plays an important role in prostaglandin synthesis and LPS-induced liver damage.

Nitric oxide (NO) produced by nitric oxide synthase (NOS) is also known to play important roles in inflammation and sepsis [6], acting as a messenger or effector molecule in a variety of tissues [7]. Inducible nitric oxide synthase (iNOS), also known as type II NOS, is not expressed under normal conditions. However,

*Correspondence to: Huei-Jane Lee, Institute of Biochemistry and Biotechnology, Chung Shan Medical University, No. 110, Sec. 1, Jianguo N. Road, South District, Taichung City, Taiwan (R.O.C.)

after exposure to endogenous and exogenous stimulators, iNOS can be quantitatively induced in various cells, including macrophages, smooth muscle cells, and hepatocytes, and triggers several disadvantageous cellular responses that cause inflammation and can lead various disorders, including sepsis and strokes [8]. Therefore, NO production by iNOS may reflect the degree of inflammation and may thereby be used to assess the effects of anti-inflammatory drugs. LPS activates iNOS in Kupffer cells, endothelial cells, and hepatocytes [9,10]. Several natural antioxidants such as curcumin [11], resveratrol [12], *Hibiscus sabdariffa* L. polyphenols (HPE) [13], and tea polyphenols [14] have been recently shown to inhibit LPS-induced iNOS and prevent hepatic damage *in vivo* [10].

A wide variety of phenolic substances from edible and medicinal plants have also been reported to have anticarcinogenic and antimutagenic activities. The majority of naturally occurring phenolics retain antioxidative and anti-inflammatory properties, which appear to contribute to their chemopreventive and chemoprotective activities [15]. Apples are abundant in polyphenols and contain a complex mixture of procyanidin, epicatechin, catechin, p-coumaroyl quinic acid, chlorogenic acid, rutin, and phloridzin. The procyanidins epicatechin and catechin are the most studied polyphenols [16] and reportedly have anti-allergic [17] anti-hyperlipidemic [18], anti-oxidant [19], and anti-tumor properties [20]. In this study, we investigated the anti-inflammatory effects of apple polyphenols AP.

MATERIALS AND METHODS

Chemicals

AP was purchased from Asahi Co. (Japan). LPS (endotoxin from *Escherichia coli*, serotype 0127:B8), alanine aminotransferase (ALT), and aspartate aminotransferase (AST) analysis kits and other chemicals were purchased from Sigma Chemical Co. (St. Louis, Mo, USA).

Animal Treatment

Male Sprague–Dawley (SD) rats (260 ± 10 g) were purchased from the National Laboratory Animal Breeding and Research Center (Taipei, Taiwan). All animals were housed in laboratory conditions (18°C–23°C, 55%–60% humidity, 12-h light/12-h dark cycle)

for at least 1 week before experimentation. Animal studies were conducted according to the guidelines for care and use of laboratory animals and were approved by the Institute of Animal Care and Use Committee (IACUC) of Chung Shan Medical University. Rats were provided food and water *ad libitum*. Rats were divided into five groups of five rats and pretreated with 50, 100, or 150 mg/kg of AP per day for 5 consecutive days by gavage. On day 5, rats were administered i.p. injections of LPS (5 mg/kg) or distilled water 1 h after AP treatment. Rats were decapitated 6 h later, and blood samples were collected for assays of ALT, AST, and alkaline phosphatase (ALKP). Livers were excised from the animals and assayed for lipid peroxidation levels and antioxidant enzyme activities, and pathological histology analyses were performed as described below. Body and liver weights were also recorded at the end of experimentation.

Hepatotoxicity Assessments

The hepatic enzymes ALT, AST, and ALKP were used as biochemical markers for early acute hepatic damage. Activities of these enzymes and biochemical values were colorimetrically determined using standard commercial kits (Sigma, St. Louis, MO).

Pathological Liver histology

After removal of livers from the animals, hepatic tissues were immediately fixed in 10% buffered formaldehyde and processed for histological examinations using conventional methods with hematoxylin and eosin (H&E) staining. Liver lesions were classified according to morphological changes, such as neutrophil infiltration. The severity of liver damage was evaluated by examining sections under 10 randomly selected high power fields ($\times 200$) and numbers of fields with lesions, and lesion areas were recorded.

Thiobarbituric acid-reacting substances

Lipid peroxidation was determined using TBARS assays according to the procedures of Yagi [21]. In these experiments, 0.5-g liver tissue samples were homogenized in 5 ml of RIPA buffer containing 1% NP-40, 50 mM Tris-base, 0.1% SDS, 0.5% deoxycholic acid, 150 mM NaCl, (pH 7.5), 10 $\mu\text{g/ml}$ leupeptin, 10 $\mu\text{g/ml}$ PMSF, and 17 $\mu\text{g/ml}$ sodium orthovanadate and centrifuged at $1000\times g$ for 30 min to obtain supernatants. Subsequently, 0.3-ml aliquots of supernatants were added to 0.3 ml of TBA (1% thiobarbituric acid

in 0.3% NaOH), and the mixture was allowed to react for 40 min at 95°C in the dark. After the reaction, samples were analyzed using a Hitachi F2000 spectrophotofluorimeter with excitation and emission wavelengths of 532 and 600 nm, respectively. TBARS concentrations were expressed as equivalents of the standard 1,1,3,3,-tetraethoxypropane (TEP).

Catalase Assay

Catalase activity in rat liver homogenates was assayed according to previously described methods [22]. In brief, homogenates (20 µl) were added to 980 µl of H₂O₂ solution containing 30 µl of ddH₂O, 50 ml of Tris-HCl-EDTA, (pH 8.0), and 900 µl of 10-mM H₂O₂. After 10 s at room temperature, the optical density of H₂O₂ was recorded at 240 nm for 1 min using a spectrophotometer. A unit of catalase activity was defined as H₂O₂ consumed/mg protein.

Determination of GSH contents

We determined liver GSH contents according to the method of Hissin and Hilf [23]. Stock solutions of the fluorescent probe o-phthalaldehyde (OPT) were freshly prepared in methanol (1 mg/ml). Homogenates were mixed with OPT and incubated for 15 min in the dark. Subsequently, we monitored fluorescence intensity at excitation and emission wavelengths of 350 and 420 nm, respectively. A GSH calibration curve was established using GSH standard, and GSH concentrations were expressed as µg GSH/mg protein.

Statistical Analysis

Data are reported as means ± standard deviations from three determinations. Differences were

identified using one-way ANOVA. $P < 0.05$ was considered significant.

RESULTS

Effects of AP on LPS-induced Hepatic Inflammation in Rats

The effects of APs on LPS-induced hepatic inflammation were examined in Sprague-Dawley rats. In these experiments, AP ameliorated LPS-induced hepatic damage in rats (Table 1). In particular, 6 h after LPS injections, plasma AST and ALT levels were significantly lower in rats that were pretreated with 150 mg/kg AP for 5 consecutive days than in control group rats. After pretreatments with AP for 5 consecutive days before LPS induction, ALPK, another index of hepatic inflammatory, also decreased (Table 1). Pretreatments with 150 mg/kg AP had no effect on liver and body weight (data not shown).

Effects of AP on LPS-induced Hepatic Lesions in Rats

The effects of AP on LPS-induced histopathological changes in rat livers were evaluated. Liver sections from the control group exhibited no inflammatory cells or cellular damage (Figure 1A). However, 6 h after LPS injections, liver lesions were observed with inflammatory neutrophil infiltration (Figure 1C). In the 10 randomly selected high power fields (×200), lesions with areas of more than half of the field were observed. These LPS induced lesions were significantly smaller (less than half of the field) and were observed in only a few AP-pretreated rats (Figure 1D, E, and F).

Table 1. Effect of apple polyphenol in LPS-induced liver inflammation

Treatment		Parameters in serum		
Apple polyphenol (mg/kg)	LPS (5 mg/kg)	ALT (IU/L)	AST (IU/L)	ALPK (IU/L)
--	--	65.8 ± 7.9	279.5 ± 36.2	275.3 ± 21.8
--	+	91.2 ± 10.3 ^a	381.4 ± 43.9 ^a	469.2 ± 46.5 ^a
50	+	80.6 ± 12.8	326.1 ± 31.7	383.1 ± 37.2 ^b
100	+	76.7 ± 10.9 ^b	297.6 ± 29.7 ^b	325.4 ± 38.1 ^b
150	+	69.5 ± 8.4 ^c	281.3 ± 31.1 ^b	291.1 ± 29.6 ^c

Data are mean ± S.D., n = 5.

Statistical significance analyzed by one-way ANOVA analysis.

^a $P < 0.01$, compared with the normal group.

^b $P < 0.05$, ^c $P < 0.005$, compared with the LPS group.

Effects of AP on LPS-induced Lipid Peroxidation in Rats

Table 2 shows comparisons of LPS-induced lipid peroxidation in livers using MDA as standard. Pretreatment with AP significantly decreased MDA levels in livers from LPS-injected rats (Table 2).

Effects of AP on LPS-induced Hepatic Antioxidant Enzyme Activities

Decreased GSH levels and antioxidant enzyme

activities have been demonstrated following LPS treatments [24]. Therefore, we investigated the effects of HPE on LPS-induced GSH levels and catalase activities. After treatment with 5 mg/mL LPS for 6 h, rat hepatic GSH levels and catalase activities decreased. Pretreatments with HPE for 5 days before LPS injections caused dose-dependent increases in GSH levels and catalase activities in rats (Table 2).

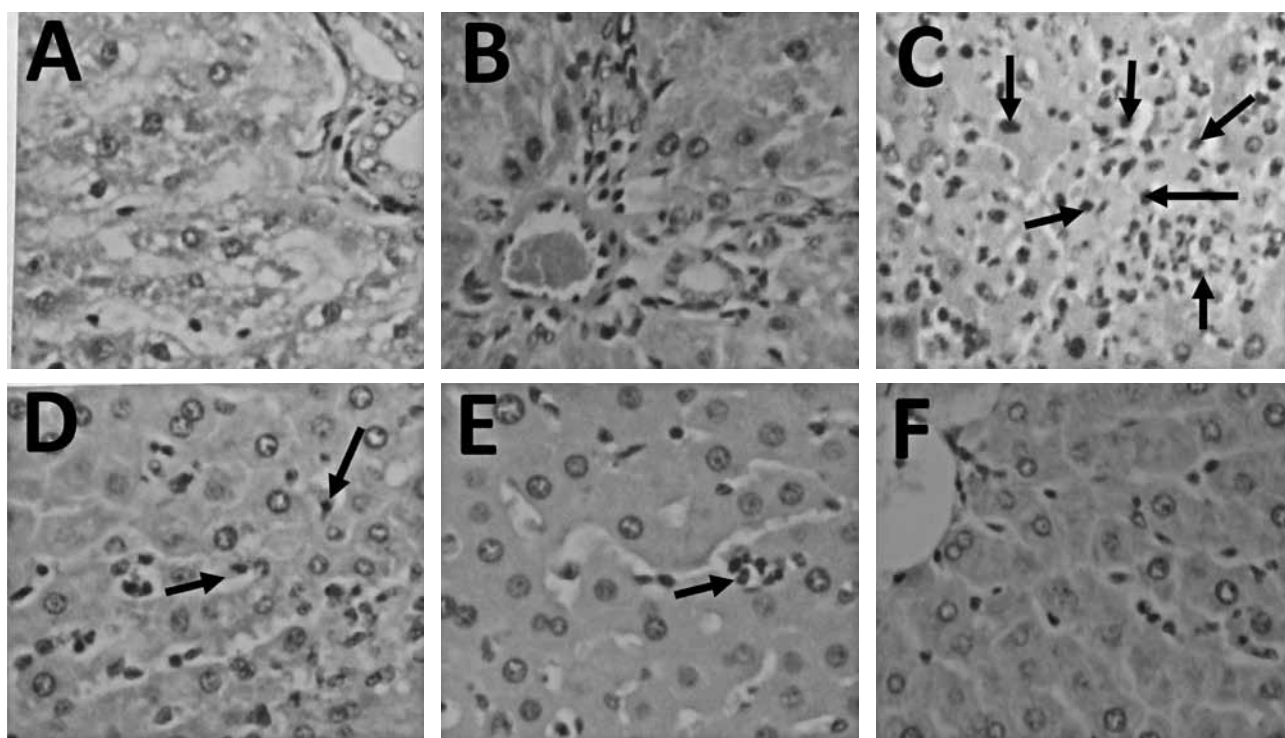


Fig. 1 Effects of Apple Polyphenol on LPS-Induced Hepatic Injury in Rats. A, normal; B, 200 mg/kg apple polyphenol; C, treated with 5 mg/kg of LPS; D, 50 mg/kg of apple polyphenol and LPS; E, 100 mg/kg of apple polyphenol and LPS; F, 200 mg/kg of apple polyphenol and LPS. Arrows point out are inflammatory neutrophils. The results were evaluated by examining the section under ten randomly selected high power fields ($\times 200$)

Table 2. Effect of apple polyphenol in LPS-induced oxidative status

Treatment		Parameters in serum		
Apple polyphenol (mg/kg)	LPS (5 mg/kg)	MDA (nmol/mg protein)	Catalase (units/mg protein)	GSH (ng/mg protein)
--	--	61.8 \pm 3.8	1367.1 \pm 252.3	5.1 \pm 0.6
--	+	89.2 \pm 9.6 ^a	735.6 \pm 179.8 ^a	3.1 \pm 0.5 ^a
50	+	78.5 \pm 10.8	892.6 \pm 203.6	3.3 \pm 0.4 ^b
100	+	72.1 \pm 9.0 ^b	1123.5 \pm 289.1 ^b	3.9 \pm 0.9 ^b
150	+	61.5 \pm 7.9 ^c	1215.3 \pm 305.3 ^b	4.7 \pm 1.0 ^b

Data are mean \pm S.D., n = 5.

Statistical significance analyzed by one-way ANOVA analysis.

^a P < 0.01, compared with the normal group.

^b P < 0.05, ^c P < 0.005, compared with the LPS group.

DISCUSSION

Despite current medical and surgical advances, hepatic failure due to sepsis remains a cause of high mortality [25,26]. Hepatic damage is primarily mediated by endotoxins of gram-negative bacteria such as LPS. The liver plays a central role in this process by clearing LPS from the serum [27]. Within the liver, LPS is sequestered by LPS binding proteins that facilitate its transfer to CD14 receptors on the surfaces of Kupffer cells. Macrophage activation by bacterial lipopolysaccharide (LPS) promotes the secretion of proinflammatory cytokines such as tumor necrosis factor- α (TNF- α) and interleukin-1 β (IL-1 β) and secretion of secondary mediators such as leukotrienes and prostaglandins (PGs). These substances are important regulators of both innate and adaptive immunity. However, their uncontrolled expression can cause acute and chronic inflammation and can lead to septic shock syndrome, which is characterized by fever, hypotension, disseminated intravascular coagulation, and multiple organ failures. Moreover, LPS-induces iNOS and cyclooxygenase-2 expression in rat livers, and the cyclooxygenase enzyme possesses both cyclooxygenase and peroxidase functions. Prostaglandins formed by cyclooxygenase impair immune surveillance and modulate proliferation in a variety of cell types [28], and the peroxidase function contributes to procarcinogen activation [29]. In addition, during infection and inflammation, high NO production has been shown to cause DNA damage and mutation *in vivo* [30]. Furthermore, cyclooxygenase and iNOS overexpression may be intimately involved in the pathogenesis of colon cancer [31], multiple sclerosis, neurodegenerative diseases, and heart infarctions [32].

A wide variety of phenolic substances are present in dietary and medicinal plants and possess striking antioxidant and anti-inflammatory properties, which to some extent contribute to their cancer chemopreventive potential. In previous studies, we demonstrated the presence of various polyphenols with antioxidant potential in *Hibiscus sabdariffa L.* extracts. We also confirmed that HPE possesses antioxidant activity *in vitro* and demonstrated inhibition of LPS-induced NO and prostaglandin E2 production and cyclooxygenase-2 and iNOS protein expression in macrophages [13]. In the present study, we demonstrated anti-inflammatory activities of AP during

LPS-induced hepatic damage *in vivo*. After injections of LPS, AST, ALT, and ALKP were increased in the plasma. However, 5-day oral pretreatments with AP reduced the induction of these inflammatory markers by LPS. Furthermore, AP inhibited LPS-induced hepatic neutrophil infiltration, suggesting that AP may contribute to the prevention of inflammation and cancer.

Activation of NF κ B is necessary for LPS-induction of iNOS and COX-2 promoters [33,34]. NF κ B comprises two proteins, p50 and p65. Following exposure to pro-inflammatory stimuli, I κ B is phosphorylated, ubiquitinated, and degraded, resulting in liberation of NF κ B dimers, translocation to the nucleus, and transcription of target genes. In particular, JNK and p38 MAPK are known key players in LPS-induced signal transduction through NF κ B. In further studies, assessments of liver JNK and p38 MAPK activation will further clarify the anti-inflammatory mechanisms of AP.

In summary, we observed that AP reduces liver inflammation and damage and improves endogenous antioxidant status following LPS injections. The present data demonstrate antioxidant effects of AP that limit the induction of inflammatory factors. However, the precise anti-inflammatory mechanisms remain unknown.

References

1. Tabas I, Glass CK: Anti-Inflammatory Therapy in Chronic Disease: Challenges and Opportunities. *Science* 2013; 339: 166-72.
2. Nowarski R, Gagliani N, Huber S, Flavell RA: Innate Immune Cells in Inflammation and Cancer. *Cancer Immunol Res* 2013; 1: 77-84.
3. Barrios-Rodiles M, Tiralocche G, Chadee K: Lipopolysaccharide modulates cyclooxygenase-2 transcriptionally and posttranscriptionally in human macrophages independently from endogenous IL-1 β and TNF- α . *J Immunol* 1999; 163: 963-9.
4. Meade EA, Smith WL, DeWitt DL: Differential inhibition of prostaglandin endoperoxide synthase (cyclooxygenase) isozymes by aspirin and other non-steroidal anti-inflammatory drugs. *J Biol Chem* 1993; 268: 6610-4.
5. Dinchuk JE: Renal abnormalities and an altered inflammatory response in mice lacking cyclooxygenase II. *Nature* 1995; 378: 406-9.
6. Wheeler AP, Bernard GR: Treating patients with severe sepsis. *New Eng J Med* 1999; 340: 207-14.
7. Lowenstein CJ, Hill SL, Lafond-Walker A, Wu J, Allen G, Landavere M, et al: Nitric oxide inhibits viral replication in murine myocarditis. *J Clin Invest* 1996; 97: 1837-43.

8. Duval DL, Miller DR, Collier J, Billings RE: Characterization of hepatic nitric oxide synthase: identification as the cytokine-inducible form primarily regulated by oxidants. *Mol Pharmacol* 1996; 50: 277-84.
9. Rockey DC, Chung JJ: Regulation of inducible nitric oxide synthase in hepatic sinusoidal endothelial cell. *Am J Physiol* 1996; 271: G260-7.
10. Zhang C, Walker LM, Hinson JA, Mayeux PR: Oxidant stress in rat liver after lipopolysaccharide administration: effect of inducible nitric oxide synthase inhibition. *J Pharmacol Exp Ther* 2000; 293: 968-72.
11. Brouet I, Ohshima H: Curcumin, an anti-tumor promoter and anti-inflammatory agent, inhibits induction of nitric oxide synthase in activated macrophages. *Biochem Biophys Res Commun* 1995; 206: 535-40.
12. Tsai SH, Lin-Shiau SY, Lin JK: Suppression of nitric oxide synthase and the down-regulation of the activation of NF- κ B in macrophages by resveratrol. *Br J Pharmacol* 1999; 126: 673-80.
13. Kao ES, Hsu JD, Wang CJ, Yang SH, Cheng SY, Lee HJ: Polyphenols extracted from *Hibiscus sabdariffa* L. inhibited lipopolysaccharide-induced inflammation by improving antioxidative conditions and regulating cyclooxygenase-2 expression. *Biosci Biotechnol Biochem* 2009; 73: 385-90.
14. Surh YJ, Chuna KS, Chaa HH, Hana SS, Keuma YS, Park KK, et al: Molecular mechanisms underlying chemopreventive activities of anti-inflammatory phytochemicals: down-regulation of COX-2 and iNOS through suppression of NF- κ B activation. *Muta Res* 2001; 480-481: 243-68.
15. Banerjee S, Rajamani P: Cellular, molecular, and biological perspective of polyphenols in chemoprevention and therapeutic adjunct in cancer. *Nature Prod* 2013; 2175-54.
16. Sugiyama H, Akazome Y, Shoji T, Yamaguchi A, Yasue M, Ohtake Y: Oligomeric Procyanidins in Apple Polyphenol Are Main Active Components for Inhibition of Pancreatic Lipase and Triglyceride Absorption. *J Agric Food Chem* 2007; 55: 4604-9.
17. Kojima T, Akiyama H, Sasai M, Taniuchi S, Goda Y, Toyoda M, et al: Anti-allergic effect of apple polyphenol on patients with atopic dermatitis: A pilot study. *Allergol Internat* 2000; 49: 69-73.
18. Hu SH, Liang ZC, Chia YC, Lien JL, Chen KS, Lee MY, et al: Antihyperlipidemic and antioxidant effects of extracts from *Pleurotus citrinopileatus*. *J Agric Food Chem* 2006; 5: 2103-10.
19. Sluis AA, Dekker M, Jager A, WMF Jongen: Activity and concentration of polyphenolic antioxidants in apple: effect of cultivar, harvest year, and storage conditions. *J Agric Food Chem* 2001; 49: 3606-13.
20. Yang KC, Tsai CY, Wang YJ, Wei PL, Lee CH, Chen IH, et al: Apple polyphenol phloretin potentiates the anticancer action of paclitaxel through induction of apoptosis in human hep G2 cells. *Mol Carcinogen* 2009; 48: 420-31.
21. Yagi K: A simple fluorometric assay for lipoperoxide in blood plasma. *Biochem Med* 1976; 15: 212-6.
22. Aebi H: Catalase. In: *Methods of enzymatic analysis*. Bergmeyer HU, editor. New York: Academic Press; 1974; pp673-84.
23. Hissin PJ, Hiff RA: Fluorometric method for determination of oxidized and reduced glutathione in tissues. *Anal Biochem* 1976; 74: 214-26.
24. Reddy MM, Mahipal SVK, Subhashini J, Reddy MC, Roy KR, Reddy GV, et al: Bacterial lipopolysaccharide-induced oxidative stress in the impairment of steroidogenesis and spermatogenesis in rats. *Reprod Toxicol* 2006; 22: 493-500.
25. Hartung T, Tiegs G, Wendel A: The role of leukotriene D4 in septic shock models. *Eicosanoids* 1992; 5: S42-4.
26. James PE, Madhani M, Roebuck W, Jackson SK, Swartz HM: Endotoxin-induced liver hypoxia: defective oxygen delivery versus oxygen consumption. *Nitric Oxide* 2002; 6: 18-28.
27. Hines IN, Wheeler MD: Recent advances in alcoholic liver disease III. Role of the innate immune response in alcoholic hepatitis. *Am J Physiol Gastrointest. Liver Physiol* 2004; 287: G310-4.
28. Marnett LJ: Aspirin and the potential role of prostaglandins in colon cancer. *Cancer Res* 1992; 52: 5575-89.
29. Eling TW, Thompson DC, Foureman GL, Curtis JF, Hughes MF: Prostaglandin H synthase and xenobiotic oxidation. *Annu Rev Pharmacol Toxicol* 1990; 30: 1-45.
30. Nguyen T, Brunson D, Crespi CL, Penman BW, Wishnok JS, Tannenbaum SR: DNA damage and mutation in human cells exposed to nitric oxide in vivo. *Proc Natl Acad Sci USA* 1992; 89: 3030-4.
31. Prescott SM, White RL: Self-promotion? Intimate connections between APC and prostaglandin H synthase-2. *Cell* 1996; 87: 783-6.
32. Good PF, Werner P, Hsu A, Olanow CW, Perl DP: Evidence for neuronal oxidative damage in Alzheimer's disease. *Am J Pathol* 1996; 149: 21-8.
33. Tseng TH, Kao ES, Chu CY, Chou FP, Lin Wu HW, Wang CJ: Protective effects of dried flower extracts of *Hibiscus sabdariffa* L. against oxidative stress in rat primary hepatocytes. *Food Chem Toxicol* 1997; 35: 1159-64.
34. Xie QW, Kashiwabara Y, Nathan C: Role of transcription factor NF-kappa B/Rel in induction of nitric oxide synthase. *J Biol Chem* 1994; 269: 4705-8.

蘋果多酚在動物模式中抑制脂多醣誘導之發炎作用

李慧禎*

中山醫學大學生化暨生物科技研究所

受文日期：民國 102 年 12 月 22 日；接受刊載：民國 103 年 1 月 8 日

摘要

背景與目的：蘋果多酚在先前文獻中被證實具有抗氧化作用，為了進一步探究其抗發炎效用，脂多醣誘導動物肝臟發炎的模式在此被施行以進行研究。

方法：蘋果多酚預先給予動物 5 天，五天後給予腹腔注射 5 mg/kg 脂多醣。6 小時後犧牲動物，測定血漿中丙胺酸轉胺酶及天門冬胺酸轉胺酶（ALT 及 AST），以及檢查肝臟組織的變化。

結果：本結果顯示在發炎模式動物中，蘋果多酚可降低血漿中 ALT 及 AST，並同時改善肝組織中的抗氧化分子，包括增加 catalase 活性及 glutathione (GSH) 含量，並減少肝臟中的脂質過氧化現象。由組織切片也發現蘋果多酚可降低肝臟中 LPS 誘導之嗜中性球浸潤的現象。

討論：目前結果暗示蘋果多酚在動物中具有抗發炎作用，並具潛力發展為抗發炎的物質。

關鍵詞：蘋果多酚、脂多醣、抗發炎

Case Report

Transient Oxygen Desaturation During Removal of A Huge Ovarian Tumor Under Intubated General Anesthesia: A Case Report

Yiu-Sion Chen^{1*}, Kuo-Sheng Huang¹, Kam-Sun Cheung¹, Kee-Ming Man¹,
Chun-Lai Ma¹, Chen-Lung Chien²

¹Department of Anesthesiology, ²Department of Gynecology, Tungs' Taichung Metro Harbor Hospital, Taichung, Taiwan

Received: Sep. 27, 2011; Accepted: Dec. 05, 2013

Abstract

Obstetric and gynecologic patients with huge abdominal or pelvic lesions often present a challenging perioperative episode to the surgeon and to the anesthesiologist. Here we report an overweight female of short stature suffering from a huge pelvic tumor requiring complete resection. During the operation, she experienced a transient decrease in blood oxygen saturation resulting from an endotracheal tube migration into the right lung, possibly due to external compression from the tumor because it was retracted and positioned against the right hemidiaphragm pushing the internal thoracic structures toward the head. The slightly head-down effect of the Trendelenburg position must also be taken into consideration. After optimal treatment, the situation was remedied, and the oxygen saturation returned to normal.

Key words: huge mass, overweight, right hemidiaphragm compression, migration, oxygen desaturation.

Introduction

Gynecologic patients with huge abdominal or pelvic lesions often present a challenging perioperative episode to the surgeon and to the anesthesiologist. The following report describes an incident of blood oxygen desaturation during the removal of a huge pelvic tumor.

A Case Report

A 58-year-old native Taiwanese woman suffered from lower abdomen discomfort and vaginal bleeding for six months before visiting our gynecology department. Physical examination revealed a huge aggressive pelvic tumor mass likely of ovarian origin.

Exploratory laparotomy with surgical removal of the tumor was performed.

On the day of surgery, she was slightly anxious and presented with a large, bulging abdomen. A review of her history revealed her to be rather healthy, apart from the illnesses mentioned above. However, she was of short stature, 143 cm in height, with a body weight of approximately 60 kg. General anesthesia was administered.

At the beginning of the surgical incision for exploratory laparotomy, the patient's vital signs were stable, and the pulse oximeter reading was 100%. Fifty minutes later, a huge cystic tumor, which was approximately the size of a soccer ball, was exposed. To continue the exploration without obscuring the interior of the lower abdomen, the huge tumor, with its connective tissue partly released and base still attached, was retracted out of the abdominal cavity and placed temporarily on the right upper abdominal quadrant. After ten minutes, the patient's pulse

*Correspondence to: Yiu-sion Chen, Department of Anesthesiology, Tungs' Taichung Metro Harbor Hospital, No.699, Sec.8, Taiwan Blvd., Wuqi Dist., Taichung City 43503, Taiwan (R.O.C.)

oximeter reading began to fall from 100% to 92%.

The anesthesia machine was fully functional, and the pipelines were intact. Suction of the endotracheal tube was performed, but no sputum was removed. Her blood pressure, electrocardiogram, and central venous pressure were normal. No rumbling heart sounds were heard, and no excessive bleeding was reported. However, breathing sounds from the left lung were diminished, and arterial blood gas data showed desaturation with a decrease in the concentration of blood oxygen (60 mmHg with $FiO_2 = 0.5$). The endotracheal tube was then retracted about fifteen millimeters away from the trachea until symmetric breathing sounds were detected from both lungs, and the surgeon was informed. The surgical assistant helped withdraw the huge tumor to reduce the compression on the upper abdomen. The patient's pulse oximeter reading then dramatically regained a normal level. The duration of the surgery was uneventful, with complete resection of the huge malignant ovarian tumor. Pathology reports revealed that huge pelvic mass weighed 4750 gm and had dimensions of $23 \times 20.4 \times 13.8$ cm (photographs shown below) and was diagnosed as a left ovary mucinous cystadenocarcinoma.

Discussion

The patient's body mass index (BMI) was 28.4, which was above the normal range and was regarded as overweight (range, 25–30), decreased respiratory reserve. The closing capacity is larger in obese

patients and likely increases the possibility of atelectasis, leading to hypoxemia in the state of general anesthesia^[3,4,6,7,11]. The application of low positive-end expiratory pressure may be a prophylaxis for respiratory preservation.

When oxygen desaturation is noted, the anesthesia machine and gas delivery system must be immediately rechecked^[12]. Sputum impaction, particularly in the case described in this report, can be catastrophic if thorough suction of these secretions is not performed abruptly because this may lead to pulmonary atelectasis^[1,2,9].

Before complete resection, it was partially extracted and placed on the right upper quadrant of the abdomen. Owing to its huge size and heavy weight, the tumor likely compressed the abdomen and pushed the right hemidiaphragm toward the patient's head, squeezing the internal thoracic contents, including the trachea, upwards. Hence, the endotracheal tube, which was fixed at the 20 cm mark, may have been forced to migrate into the straighter and direct right main bronchus. This resulted in right-sided one-lung ventilation and hypoxemia. The decrease in the pulse oximeter reading to 92% correlated with a 60 mmHg fall in oxygen tension, obtained from the arterial blood gas data. The situation was resolved by retracting the endotracheal tube until symmetric breathing sounds were detected and refixing it at 18.5 cm. The original tip of the endotracheal tube was up to the 20 cm mark, which may be very close to the carina, leading to a significant risk of endobronchial tube migration. Subsequent lifting



Fig. 1 Huge tumor being positioned at the right upper abdominal quadrant.



Fig. 2 Huge cystic tumor with size of $23 \times 20.4 \times 13.8$ cm, and weight of 4750 grams

of the huge tumor to prevent compression of the upper abdomen eliminated the force pushing against the right hemidiaphragm. This adverse condition returned to normal within five minutes after lifting the tumor from the abdomen.

The surgery was conducted in a slightly tilted Trendelenburg position, which would also be a cause for endobronchial tube migration, resulting in one-lung ventilation and hypoxemia. Venous air embolism can occur when an open vein is subatmospheric. Clinically, signs of venous air embolism are often not apparent until large amounts of air have been entrained. A decrease in end-tidal carbon dioxide or arterial oxygen saturation may be noticed before hemodynamic changes^[1,2]. In case the approach described in this study had been ineffective, more aggressive monitors such as Doppler sonography and transesophageal echocardiography would have been necessary for further differential diagnosis^[2]. Because the phase of oxygen desaturation in our patient was a short, a transient episode, more complicated incidents such as re-expansion pulmonary edema and pulmonary embolism could not be considered and therefore should be considered in such cases. Furthermore, in the surgical position described here, the abdominal contents are thrust toward the lungs, as a result of the gravitational pull, thereby increasing the chances of endotracheal tube migration into the unilateral lung, resulting in one-lung ventilation^[8]. Fortunately, our management provided a solution.

The patient initially presented with a distended abdomen due to a huge pelvic mass, which pushed up the abdominal viscera, resembling a pregnant woman. Thus, the intrathoracic contents were also displaced upwards, which decreased the respiratory reserve^[10]. As the huge tumor was resected, the bulging force waned and respiratory functions improved. However, the pitfall was that the heavy tumor mass was rested on the right upper quadrant, directing the pushing force to the right hemidiaphragm, resulting in one-lung ventilation and oxygen desaturation^[5]. More precisely, the endotracheal tube may have migrated to the endobronchium.

Conclusions

Patients suffering from an abdominal or pelvic tumor of huge size with respect to a short, obese

stature may present a very delicate respiratory pathophysiology when awake or under anesthesia^[1,4,13]. If the resected tumor has a considerable mass, it is suggested that the tumor should not be placed on the patient's body. The surgical position of the patient, particularly the Trendelenburg position, also has an impact that must be closely monitored for the maintenance of a stable physiological state during the surgery. It is important for the anesthetist and the surgeon to work closely, supported by multidisciplinary concepts. Changing surgical positions may help avoid unstable perioperative hemodynamics that are well known to be hazardous to the patient in incidents of oxygen desaturation situations during the operation^[1,14].

References

1. Miller RD: Miller's Anesthesia 7th edition. 2010 Volume I & II Churchill Livingstone.
2. Morgan GE: Clinical Anesthesiology 4th edition. 2006 McGraw Hill.
3. Salome CM: Physiology of obesity and effects on lung function. *J Appl Physiol*. 2010 Jan;108(1):206-11.
4. Zoremba M.: The influence of perioperative oxygen concentration on postoperative lung function in moderately obese adults. *Eur J Anaesthesiol*. 2010 Jun;27(6):501-7.
5. Emel C : The effects of body fat distribution on pulmonary function tests in the overweight and obese. *South Med J*. 2009, Jan 102(1)30.5.
6. Jones RL: The effects of body mass index on lung volumes. *Chest* 2006 Sep;130(3):827-33.
7. Parameswaran K : Altered respiratory physiology in obesity. *Can Respir J*. 2006May-Jun;13(4):203-10.
8. Gupta N: Tube migration during laparoscopic gynecological surgery. *J Anaesthesiol Clin Pharmacol* 2010 Oct;26(4): 537-8.
9. Hedenstierna G: Alveolar collapse and closure of airways: regular effects of anaesthesia. *Clin Physiol Funct Imaging* 2003 May;23(3):123-9.
10. Stadler DL: Abdominal compression increases upper airway collapsibility during sleep in obese male obstructive sleep apnea patients. *Sleep*. 2009 Dec;32(12):1579-87.
11. Fujinaga A: Anesthetic management of an extremely obese patient. *J Anesth*. 2007;21(2):261-4. Epub 2007 May 30.
12. Hay H: Oxygen delivery failure resulting from interference with a Bain breathing system. *Eur J Anaesthesiol*. 2000 Sep;17(9):591-3.
13. Hoffman EA: Effect of body orientation on regional lung expansion: a computed tomographic approach. *J Appl Physiol*. 1985 Aug;59(2):468-80.
14. Ezri T: The endotracheal tube moves more often in obese patients undergoing laparoscopy compared with open abdominal surgery. *Anesth Analg*. 2003 Jan;96(1):278-82.

在插管式全身麻醉下移除巨大的卵巢腫瘤時 出現渡過性血氧飽和度下降：病例報告

陳耀舜^{1*} 黃國生¹ 張錦新¹ 文寄銘¹ 馬振來¹ 簡陳榮²

童綜合醫院 ¹麻醉部 ²婦產部

受文日期：民國 100 年 9 月 27 日；接受刊載：民國 102 年 12 月 05 日

摘要

有巨大的腹部或骨盆病灶的婦科患者，經常帶給外科和麻醉醫師富有挑戰性的術中狀況。以下報告是關於一位超重且身材矮小的女性，她患有巨大骨盆腫瘤，須要作外科手術切除。在術中，她出現了肺部通氣量降低。其中是因為氣管內管移入右側肺部而導致血氧飽和度下降。這種情況是可能因為部分被移出體外的腫瘤安置在右腹部上方而造成右側橫膈之擠壓，繼續推擠內部臟腑往頭的方向所致。稍微頭低腳高的手術位置亦被考慮在內。在適當的處理以後，排除了狀況，血氧飽和度恢復正常。

關鍵詞：巨大腫瘤、超重、右側橫膈肌擠壓、移除、氧飽和度下降

Case Report

Tophaceous Gout of the Lumbar Spine: A case report

Hsin-Pai Lee¹, Se-Yuan Liu², Shih-Peng Hsieh³, Cherng-Gueih Shy⁴, Yen-Hsuan Jean^{1*}

¹Section of Orthopedic Surgery, ²Section of Surgery, ³Pathology, ⁴Radiology, Pingtung Christian Hospital, Pingtung, Taiwan

Received: Jul. 12, 2013 ; Accepted: Aug. 07, 2013

Abstract

Although gout is a common metabolic disease, spinal gout is rare. Its clinical manifestation is similar to that of lumbar spinal stenosis with radiculopathy. This case report describes the presentation of spinal gout in a 46-year-old male with a prolonged history of bilateral tophaceous gout of the large and small joints of the hands, wrists, elbows, knees, ankles, and feet, along with neurological abnormalities of the lower limbs. His radiological findings were suggestive of a degenerative process. Spinal gouty arthritis was diagnosed only after the tophi in the facets were detected during surgery and verified in a pathological examination. The histological diagnosis confirmed tophaceous gout. Surgical decompression and the subsequent optimization of pharmacological treatment enabled a good recovery from the neurological complications. Spinal surgeons should consider spinal gout when considering the differential diagnoses of patients with gout and axial pain, with or without neurological deficits.

Key words: Gout, spine, tophi, radiculopathy, surgery

Introduction

Gout is a common metabolic disorder characterized by recurrent episodes of arthritis associated with the presence of monosodium urate monohydrate crystals in the tissue or synovial fluid leucocytes^[1]. Gout, which is the most common cause of inflammatory arthritis in men aged >40 years^[2], affects 0.5%–1% of the men in western countries with a male:female ratio of 7–9:1^[3]. Gouty arthritis typically affects the distal joints of the appendicular skeleton^[4]. Patients present with varying clinical symptoms that range from back pain to acute paraparesis^[5]. Because of the rarity of this complication, the diagnosis is usually not made until proven by biopsy^[6]. Herein, we present an adult case of spinal gout, along with a review of the literature, and discuss the presenting symptoms, diagnosis, and treatment.

Case report

A 46-year-old man with a 15-year history of gout reported a 1-year history of lower back pain, left buttock pain, and numbness of the lateral aspect of the left foot, which was interfering with his ability to walk. He had a 10-year history of recurrent episodes of multiple tophi involving the ankles, knees, and the small joints of the hands, wrists, and elbows, and he had been prescribed nonsteroidal anti-inflammatory drugs (NSAIDs) as treatment. The patient had a history of episodic hyperuricemia with gouty arthritis attack. He was examined in an outpatient clinic, and NSAIDs therapy was initiated. Despite the drug therapy, the neurological symptoms in the lower limbs worsened and was admitted to our hospital. There was no history of trauma. A physical examination revealed a marked tenderness on the left side of the lower back and flank as well as numbness of the left thigh and leg. Multiple subcutaneous nodules suggesting gouty tophi were also noted in hands, elbows, and feet. Radiographs of the lumbar spine showed spondylolisthesis of L4/L5 and bilateral degenerative facet arthropathy at the L4/L5–S1 level, without any

*Correspondence to: Yen-Hsuan Jean, MD, PhD, Associate Prof. Address: Department of Orthopedic Surgery, Pingtung Christian Hospital, No. 60, Da-Lan Road, Pingtung 900, Taiwan (R.O.C.)

evidence of erosive changes (Fig. 1). Magnetic resonance imaging (MRI) of the lumbosacral spine showed a significant narrowing of the L4–S1 left lateral recess, a left facet joint abnormality in the form of a hypertrophy of the ligamentum flavum and facet joints, and posterior bulging of the L4/L5 and L5/S1 intervertebral discs (Fig. 2). In addition, we observed a hypointense plaque-like hypertrophic lesion in the ligamentum flavum along linear hyperintense material (Fig. 2). The T2-weighted images showed isolated hypointense areas within the right facet joint and a hyperintense area within the left facet joint. Laboratory studies revealed a serum uric acid level of 10.5 mg/dL and a creatinine level of 1.9 mg/dL. The results of all of the other tests, including the erythrocyte sedimentation rate, were within the respective normal ranges. Conservative treatment with the oral administration of NSAIDs and benzbromarone was combined with physical therapy, including traction, was administered because the clinical impression was L4/L5 and L5/S1 spinal stenosis with left radiculopathy. Because no definite improvement was

observed after conservative treatment for 2 months, surgical intervention was scheduled. During the operation (laminectomy), chalky white material and few vessels eroding the left L4/L5 and S1 facet joint were observed to be extruding from the left side of the L4/L5 facet joint. No pus was detected. Histological analysis revealed granulation tissue, multinucleated giant cells, and amorphous eosinophilic material with thin needle-shaped crystals that were negatively birefringent under polarized light (Fig. 3). These results were consistent with the diagnosis of monosodium urate crystals. Bacterial cultures of the specimens did not grow any microbes, and Gram staining was also negative. After surgery, 0.5 mg of colchicine was administered orally twice a day for 4 weeks. The symptoms were resolved, and the patient was symptom free at the 1-year follow-up visits.

Discussion

Gout is predominantly a disease of middle-aged men, although asymptomatic hyperuricemia is 10

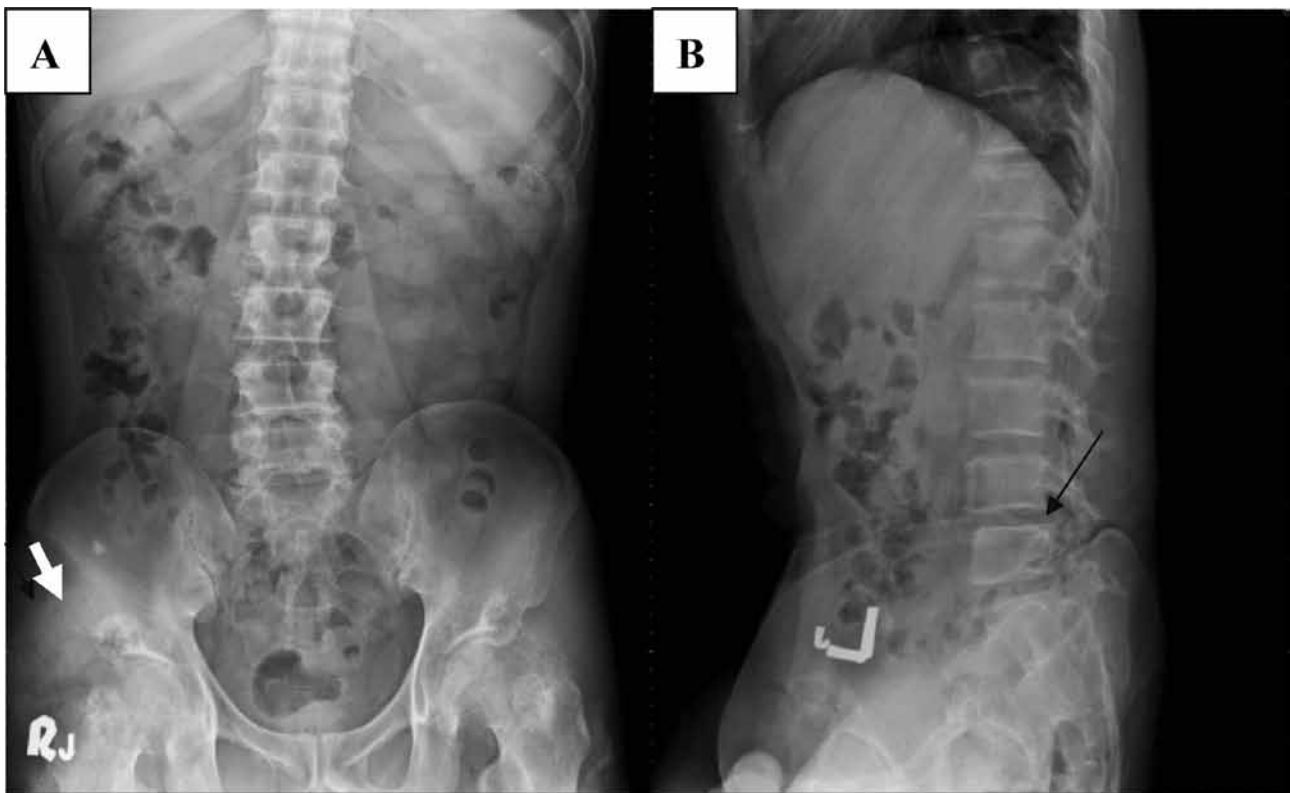


Fig. 1. Radiographs of the lumbar spine. (A) Anteroposterior view, degenerative facet arthropathy at L4/L5 and L5/S1, and multiple tophi over both hip joints (white arrow). (B) Lateral view, spondylolisthesis of L4/L5, grade 1 (black arrow).

times more common than gout^[7]. Gouty arthritis of the axial joints, particularly of the spine, is very rare^[8]. The prevalence of spinal involvement in gout is rare, although it is probably underestimated. Spinal involvement is being increasingly reported as physicians are becoming more aware of this complication. To date, over 80 cases of spinal gout have been reported in the literature, and most cases involve only the lumbar spine^[6,9-12]. Autopsy studies have

not clearly identified that gout involves the spine, despite the fact that the axial skeleton is extensively involved^[13].

The reason why this crystal deposition disease occasionally involves the spine is unknown. It has been suggested that, irrespective of the tissues affected, a previous injury or tissue necrosis is a prerequisite for urate deposition^[9]. Another report has suggested that the factors that may induce tophi formation

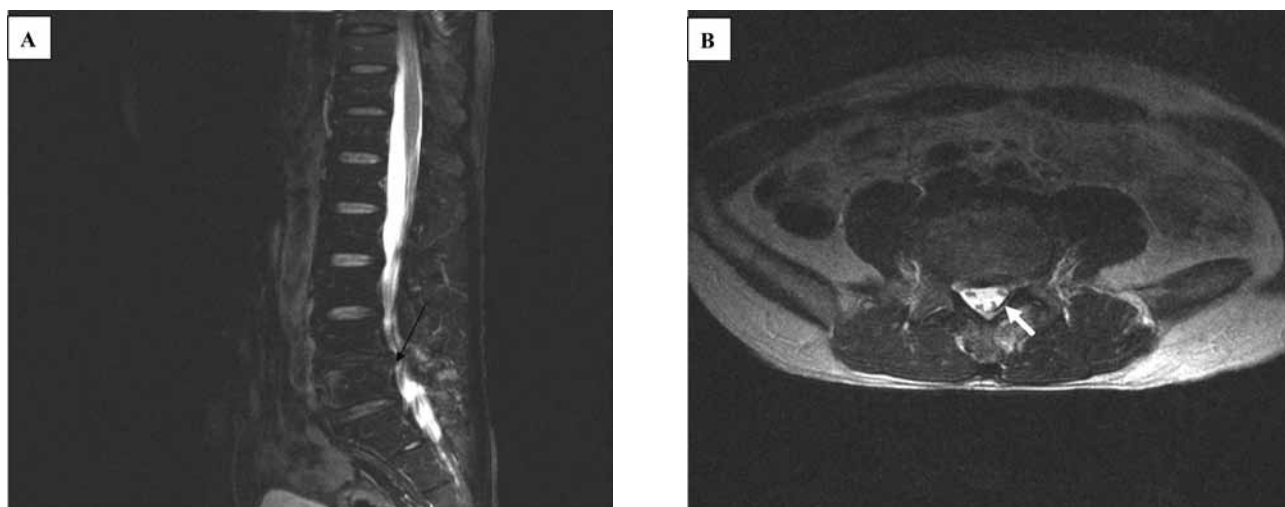


Fig. 2. (A) Magnetic resonance image (MRI) of the lumbosacral spine showing significant L4/L5 and L5/S1 left lateral recess narrowing, a left facet joint abnormality in the form of hypertrophy of the ligamentum flavum and facet joints, and bulging of the posterior disc. (B). MRI showing a hypointense plaque-like hypertrophic lesion in the ligamentum flavum along linear hyperintense material (white arrow). The T2-weighted image showed isolated hypointense areas within the right facet joint and a hyperintense area within the left facet joint.

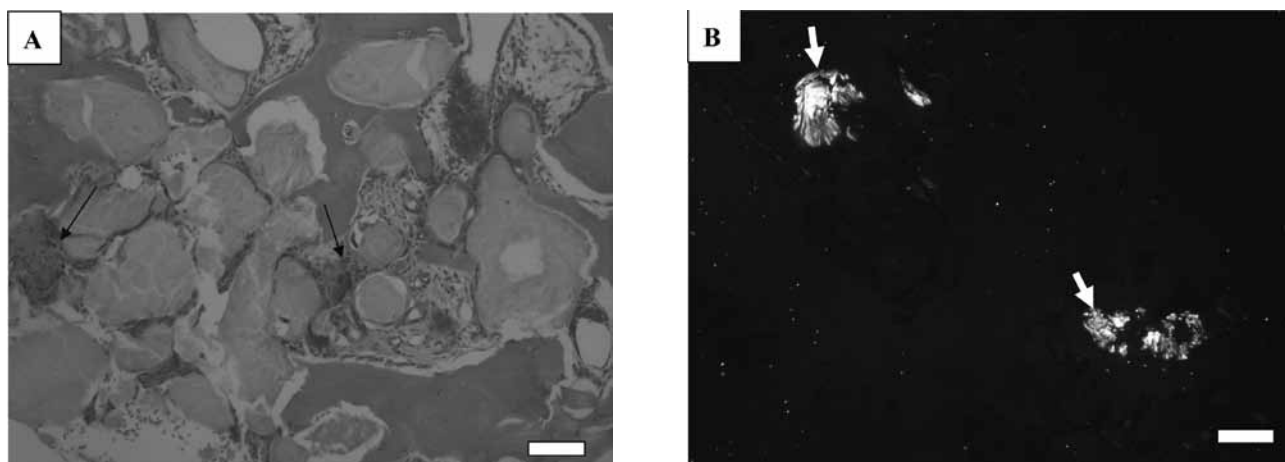


Fig. 3. Histopathology of the lumbar specimen. (A). The sections of the specimen show the ligamentum flavum with the deposition of crystalline and amorphous deposits of urate, which are surrounded by macrophages, lymphocytes, fibroblasts, and multinucleated giant cells (arrow). The findings are consistent with those of tophi. Hematoxylin and eosin stain, original magnification 200 \times . (B). Histological examination showing granulation tissue with a focus on pale-to-bluish amorphous linear needle-like crystallized material, which was negatively birefringent under polarizing microscopy and highly suggestive of tophaceous gout (white arrow) (Scale bar = 200 μ m).

include low temperature, decreased pH, and binding to plasma protein^[14]. Degenerative diseases of the spine may also be a predisposing factor, because most cases involving the lumbar spine predominate at the lumbosacral junction^[15]. Serum uric acid levels vary greatly from normal to markedly high, and thus are not reliable for establishing a diagnosis of gout^[16]. Plasma urate levels >7 mg/dL are considered increased, because this exceeds the saturation level for urate solubility at normal body temperature and normal blood pH^[3]. In our case, despite a 10-year history of recurrent episodes of gout, the patient had no history of trauma to the lumbar spine. He did have a history of hyperuricemia, and the uric acid level was high at admission (10.6 mg/dL). The spondyloitic inflammatory changes may have been the main factors that induced the deposition of urate crystals in the present case; however, the mechanism underlying the accumulation of urate crystals in the facet joints remains unclear.

Tophi may occur in the spine, including the intervertebral discs, ligament flavum, facet joints, lamina, pedicles, extradural soft tissues, and filum terminale^[1,6,10]. The clinical presentation of spinal gout ranges from isolated neck or back pain to various neurological syndromes, including radiculopathy, myelopathy, and the cauda equina syndrome^[17]. The mechanism of compression varies according to the vertebral level^[1,17,18]. In the lumbar region, which is most frequently affected, radicular compression is linked to the massive infiltration of ligaments by gouty tophi^[18]. Serial imaging of patients with gout has shown that large tophi can form quickly within months^[19]. These rapidly growing lesions may cause symptoms of spinal cord compression and neurological compromise^[9]. Urate crystal deposition in the vertebral joints may be considered an extension of the articular involvement of the peripheral joints, although its incidence remains unknown.

Radiographic abnormalities of spinal gouty arthropathies are nonspecific and include disc space narrowing with ill-defined erosion of the vertebral endplates and bony destruction. The MRI appearance of tophaceous gout of the spine is quite variable^[20]. On MRI scans, tophaceous deposits in the spine produce abnormal signals on both T1-weighted and T2-weighted images that are enhanced with gadolinium administration^[20-22]. One report has shown that gouty tophi on MRI are isointense with

muscle on T1-weighted images and have a low-to-intermediate signal intensity on T2-weighted images with homogeneous enhancement^[21]. Another study has suggested that the very hyperintense lesions that are observed on T2-weighted images are caused by the high protein content in the amorphous center of the tophi^[22]. However, the hypointensities on T2-weighted imaging may represent calcification, mature fibrous tissue, and urate crystals^[13]. Even though MRI cannot definitively diagnose spinal gout, it may aid in the diagnosis of this disorder relative to other possible conditions, such as degenerative, inflammatory, infectious, or neoplastic processes. In the present case, sagittal T1-weighted images showed isointense-to-hypointense signals within the right facet joint, and the T2-weighted images showed a hyperintensity within the right facet joint (Fig. 2). To date, we could not find any other case reports in the literature in which patients with spinal gout were diagnosed with a baseline MRI of the spine. However, if gout is suspected and if neurological symptoms that necessitate decompressive surgery are absent, a computer tomography-guided fine-needle biopsy procedure can easily establish the diagnosis^[23].

Pharmacological treatment with allopurinol and NSAIDs should be optimized in order to obviate the need for surgery^[2]. Maintaining a high fluid intake and using alkalinizing agents may limit the precipitation of uric acid and its sequelae^[19]. Decompression surgery is probably the treatment of choice for acute neurological compromise, and it is indicated when conservative treatment fails. However, the medical treatment of spinal gout with steroids may be effective if the nature of the cord compression is acute intense inflammation, as in acute synovitis in a gouty attack affecting a peripheral joint^[13,15]. In the present case, surgery was performed because of the failure of conservative treatment, and the symptoms subsided postoperatively.

The histological features of tophaceous gout include granuloma formation with multinucleated giant cells, histiocytes, and fibroblasts surrounding amorphous acellular material^[19]. The material that is obtained at biopsy must be preserved in 100% alcohol if gout is suspected because monosodium urate is soluble in formalin^[23]. If the specimen is treated with formalin, it will lead to the absence of birefringent crystals that are visualized under polarized light. It is important to clearly communicate with

the surgeon about this diagnostic possibility so that the specimen is properly fixed^[19]. Some reported cases of spinal gout have symptoms that mimic spinal infection or metastasis^[1,21]. They had an acute onset of fever and lower back pain with neurological deficits. The diagnosis can only be confirmed by a histological examination of the tissues that are removed during surgical decompression. A high index of suspicion can help clinicians make the correct diagnosis in patients with clinical features, particularly hyperuricemia and peripheral gouty involvement. During the operation on our present case, the white chalky material extruding from the left facet joint indicated that gouty tophi were likely (Fig. 3), and we therefore soaked the material with alcohol instead of formalin. Other granulomatous conditions, including tuberculosis and fungal infections, should also be considered in the differential diagnosis.

In conclusion, although rare, gouty arthropathy of the lumbar spine should be considered in all patients with neurological symptoms and known or suspected gout. Surgical decompression is indicated if conservative treatment fails to reverse the neurological dysfunction. Spinal gout should be included in the differential diagnoses of patients with back pain or neurological symptoms.

References

1. A. Greenspan. Miscellaneous arthritides: Gout. In: Greenspan A, ed. *Orthopedic radiology: a practical approach*, 2nd ed. Philadelphia, USA: Lippincott, (1997) 14.8-14.10.
2. King JC, Nicholaas C. Gouty arthropathy of the lumbar spine: a case report and review of the literature. *Spine* 1997;22:2309-2312.
3. Terkeltaub R. Gout. *N Eng J Med* 2003;349:1647-1655.
4. Konatalapalli RM, Demarco PJ, Jelinek JS, Murphey M, Gibson M, Jennings B, et al. Weinstein. Gout in the axial skeleton. *J Rheumatol* 2009;36:609-613.
5. Blasco JLS, Sarro NV, Marnov A, Martin JJA. Cervical cord compression due to intradiscal gouty tophus. *Spine* 2012; 37:E1534-1536.
6. Fraser JF, Anand VK, Schwartz TH. Endoscopic biopsy sampling of tophaceous gout of the odontoid process. Case report and review of the literature. *J Neurosurg Spine* 2007;7: 61-64.
7. Sabharwal S, Gibson T. Cervical gout. *Br J Rheumatol* 1988;27:413-414.
8. Kotake S, Nanke Y. Spinal tophaceous gout. *Intern Med* 2012;51:237-238.
9. Hsu CY, Shih TF, Huang KM, Chen PQ, Sheu JJ, Li YW. Tophaceous gout of the spine: MR imaging features. *Clin Radiology* 2002;57:919-925.
10. Fentenot A, Harris P, Macasa A, Menon Y, Quinet R. An initial presentation of polyarticular gout with spinal involvement. *J Clin Rheumatol* 2008;14:188-189.
11. Tsai CH, Chen YJ, Hsu HC, Chen HT. Bacteremia coexisting with tophaceous gout of the spine mimicking spondylodiscitis. *Spine* 2009;34: E106-109.
12. Yamamoto M, Tabeya T, Masaki Y, Suzuki C, Naishiro Y, Ishigami H, et al. Tophaceous gout in the cervical spine. *Intern Med* 2012;51:325-328.
13. Cabot J, Mosel L, Kong A, Hayward M. Tophaceous gout in the cervical spine. *Skeletal Radiol* 2005;34:803-806.
14. Yen HL, Cheng CH, Lin JW. Cervical myelopathy due to gouty tophi in the intervertebral disc space. *Acta Neurochir (Wien)* 2002;44:205-207.
15. Bonaldi VM, Duong H, Starr MR, Sarazin LL, Richardson J. Tophaceous gout of the lumbar spine mimicking an epidural abscess: MR features. *AJNR Am J Neuroradiol* 1996;17:1949-1952.
16. Hadler MM, Franck WA, Bress NM, Robinson DR. Acute polyarticular gout. *Am J Med* 1974; 56:715-719.
17. Murshid WR, Moss TH, Ettles DF, Cummins BH. Tophaceous gout of the spine causing spinal cord compression. *Br J Neurosurg* 1994;8:751-754.
18. Varga J, Giampaolo C, Goldenberg DL. Tophaceous gout of the spine in a patient with no peripheral tophi: case report and review of the literature. *Arthritis Rheum* 1985;28:1312-1315.
19. Draganescu M, Leventhal LJ. Spinal gout: case report and review of the literature. *J Clin Rheumatol* 2004;10:74-79.
20. Kuo YJ, Chiang CJ, Tsuang YH. Gouty arthropathy of the cervical spine in a young adult. *J Chin Med Assoc* 2007;70:180-182.
21. Duprez D, Malghem J, Vande Berg BC, Noel HM, Munting EA, Maldague BE. Gout in the cervical spine: MR pattern mimicking discovertebral infection. *Am J Neuroradiol* 1996;17:151-153.
22. Saketkoo LA, Robertson HJ, Dyer HR, Virk ZU, Ferreyro HR, Espinoza LR. Axial gouty arthropathy. *Am J Med Sci* 2009;338:140-146.
23. Kaye PV, Dreyer MD: Spinal gout: an unusual clinical and cytological presentation. *Cytopathology* 1999;10:411-414.

腰椎痛風性關節炎：一病例報告

李心白¹ 劉思源² 謝時鵬³ 施承貴⁴ 簡言軒^{1*}

¹屏東基督教醫院骨科 ²外科部 ³病理科 ⁴放射科

受文日期：民國 102 年 07 月 12 日；接受刊載：102 年 08 月 07 日

摘要

痛風乃一常見代謝性疾病，但脊椎的痛風仍屬少見，其臨床表徵和脊椎狹窄症併神經根壓迫類似。此病例報告描述一 46 歲男性罹患全身多處關節如手指、腕、肘部、膝、踝及足部皆有痛風石，另下肢亦有神經壓迫症狀，放射線檢查顯示有腰椎狹窄症，其脊椎痛風性關節炎是在手術中肉眼及組織病理切片証實。該病患經由手術減壓和適當的痛風藥物治療後已達良好的療效。脊椎外科醫師在面對脊椎疾病處置時，應把痛風列入鑑別診斷之一，以達正確的治療。

關鍵詞：痛風、脊椎、痛風石、神經根壓迫、外科手術

Case Report

以核磁共振早期診斷日本腦炎之病例報告

高崇智^{1*} 李佳茹² 遲景上¹ 古劉愛敏¹ 蔡青劭^{2,3} 高佳慧¹童綜合醫療社團法人童綜合醫院 兒童醫學部¹ 醫研部² 耳鼻喉科³

受文日期：民國 102 年 5 月 28 日；接受刊載：民國 102 年 8 月 23 日

摘要

在東亞洲及南亞洲，日本腦炎是一個最重要的病毒性腦炎。本院於 2010 年 7 月經歷一名 1 歲 4 個月大幼童，主訴咳嗽有痰及流鼻水，伴隨發燒已 7 天，5 天內反覆全身僵直痙攣，意識不清，經腦部 MRI 檢查與日本腦炎之 IgM 抗體效價四倍增加診斷為日本腦炎。日本腦炎的診斷包括季節性、居住地區、流行地區工作或旅遊史、蚊蟲叮咬、疫苗接種、臨床表徵、血清學檢查與腦部 MRI 檢查等。多篇文獻指出典型之腦部 MRI 特徵有助於早期診斷，因此當病患出現發燒、頭痛、意識不清，且腦部 MRI 出現特徵性丘腦病變，須高度懷疑為日本腦炎。而接種日本腦炎疫苗是最直接有效的預防方法。

關鍵詞：日本腦炎、核磁共振影像、日本腦炎抗體

前言

日本腦炎是一種以蚊子為媒介的傳染疾病，致病原為日本腦炎病毒 (Japanese encephalitis virus)，屬於黃病毒科的病毒 (Flaviviridae)。在臺灣，傳播日本腦炎的主要病媒蚊有三種，分別為三斑家蚊 (*Culex tritaeniorhynchus* Giles)、環紋家蚊 (*Cx. annulus* Theobald) 及白頭家蚊 (*Cx. fusciocephala* Theobald)。豬可被日本腦炎病毒感染引起病毒血症但不會發病，稱為增幅宿主，所以豬為病媒蚊感染人類重要的病源。從 1968 年起台灣地區即對 2 歲幼童展開二劑疫苗全面預防接種；1974 年則在二劑基礎接種外，於隔年再追加一劑；1983 年再增加國小一年級的追加接種。1983 年以後接種政策是凡滿一歲三個月大的幼童接種第 1 劑，二星期後再接種第 2 劑，一年以後追加接種第 3 劑，國小一年級再追加接種第 4 劑^[1]。在 1976 年以後，10 歲以下兒童的確定病例發生率已逐漸下降，1998 年以後，20 歲以上確定病例佔 93%^[2]，顯示病例已以成人為主。本病例報告為 1 歲 4 個月大幼童，經診斷為日本腦炎，在國內有關嬰幼童日本腦炎的文獻並不多，特提出報告，並加以討論。

病例報告

病患為 1 歲 4 個月大幼童，2010 年 7 月至本院急診室就診，主訴咳嗽有痰及流鼻水，伴隨發燒已 7 天，5 天內反覆全身僵直痙攣，意識不清，曾至其他醫院就診，未見好轉，於是到本院就診。轉至本院時已呈現昏迷狀態，故送小兒加護病房照護。病患於他院曾抽取腦脊髓液檢查，白血球數為 50 U/L、紅血球數為 3410 U/L、中性球為 21%、淋巴球為 55%。本院安排病人接受腦波、腦部核磁共振影像 (magnetic resonance imaging; MRI) 及抽血檢查，腦波報告顯示病患腦波變慢，大腦嚴重功能不全，懷疑為代謝性腦病、腦損傷或腦炎；腦部 MRI 顯示 (圖 1)，在 T2 影像雙側腦丘 (thalamus)、左側尾核 (caudate)、黑質 (substantial nigra) 及腦迴 (gyrus) 頭尾均有高訊號與細胞毒性水腫，但未傷害到內部腦囊及雙側基底節；MRS (magnetic resonance spectroscopy) 顯示乳酸出現減少了 NAA (N-acetyl Aspartate) 訊號；血清學檢查方面，單純疱疹病毒 (Herpes simplex virus; HSV) 之 IgG 與 IgM 抗體皆為陰性，日本腦炎之 IgM 抗體效價有四倍增加^{註 1}。根據腦部 MRI 檢查與日本腦炎之 IgM 抗體效價四倍增加診斷為日本腦炎。住院第一天在尚未確診日本腦炎前，先以廣效性抗生素使用 Augmentin、Zovirax 及減少腦部發炎的

* 通訊作者：高崇智醫師 童綜合醫療社團法人童綜合醫院 兒童醫學部 43503 臺中市梧棲區臺灣大道八段 699 號

類固醇 Methylprednisolone 治療，隔天改用 Rocephin 治療腦炎。病人總共住院 20 天。經過治療後，症狀及徵象好轉，生命特徵相對穩定即出院，但因病人仍無法進食故出院時插著鼻胃管。因日本腦炎造成病患四肢無力及語言發展不全，持續於復健科門診追蹤。

討 論

在東亞洲及南亞洲，日本腦炎是一個最重要的病毒性腦炎^[3]。在台灣尚未施打疫苗的年代，兒童是主要病患，但近年來都是以成人發病為主，最近五年以來，每年的確定病例數約於 10 至 30 例之間^[2]。在台灣主要流行季節集中於每年 5 至 10 月，高峰期通常出現在 6-7 月，因此幼童常規日本腦炎疫苗接種都集中於每年 3 至 5 月。本病例並未施打日本腦炎疫苗屬高危險群。根據許麗卿等人^[1]的報告指出，3~6 歲幼童完成三劑疫苗接種者，中和抗體陽性率為 67%，接種二劑者為 66%，接種一劑者為 33%，未接種疫苗者為 40%，顯示雖然自然感染率高，但接受二劑以上疫苗者仍具較高保護力，因此接種日本腦炎疫苗是最直接有效的預防方法。

病患被蚊子叮咬後，經過約 4~14 天的潛伏期，初期症狀類似感冒，包括有發燒、頭痛、疲倦、咳嗽、噁心、嘔吐、食欲不振、腹痛與感覺異常等非特異性症狀，易被誤診而延誤。也因沒有特殊的臨床表現，所以單獨以臨床表現很難與其他的急性疾病如單純疱疹腦炎做區別。利用以下三種方法可達到最好的診斷：自腦脊液中培養日本腦炎病毒、偵測日本腦炎抗原、及利用反轉錄聚合酶連鎖反應 (RT-PCR) 測定日本腦炎病毒 RNA。血清學檢驗是日本腦炎檢驗最主要的方法，可

利用酵素免疫法 (enzyme-linked immunosorbent assay; ELISA) 測定成對血清中日本腦炎 IgM 或 IgG 抗體有四倍或更高倍上升^[4]；也可運用血球凝集抑制試驗 (hemagglutination inhibition; HI) 或補體中和試驗 (complement fixation) 偵測血清中 IgM 及 IgG 抗體。但血清學檢查至少有 7 天等待期且有許多限制並須要成對血清，故無法做為早期診斷^[5-6]。衛生福利部疾病管制署對急性期血清或 CSF 檢體會採用 RT-PCR 及 ELISA 進行檢驗，恢復期血清會採用 ELISA 檢驗。RT-PCR 陽性的檢體會進行病毒分離。

MRI 在腦炎可做為偵測損傷及損傷程度的工具，也可用來確認或排除特定診斷。來自日本腦炎流行區域的腦炎病人，若由 MRI 發現兩側腦丘損傷須高度懷疑為日本腦炎^[7]。在日本腦炎病患腦部 MRI 常出現特徵性腦丘病變，包括在 T1 影像有低程度 (hypointense) 損傷，在 T2 影像有高精度 (hyperintense) 損傷^[3,8-9]。在 Kalita 等人^[8]的研究報告中，日本腦炎病人電腦斷層掃描 (computed tomography; CT) 的不正常率為 55.3%，而 MRI 則全都出現不正常，其中腦丘損傷有 94%、基底節 35.5%、中腦 58%、橋腦 19%、小腦 25.8% 及大腦皮質 19%。由此可知，在腦丘與腦丘以外的異常，MRI 的敏感度高於 CT。此論點在其他研究報告中也有相同結論^[3,10]。典型腦部 MRI 檢查結果有助於早期診斷，也可縮短等待時間及避免使用不必要的藥物^[11]。

MRS 是利用磁振原理研究活體腦內組織代謝產物的定性與定量變化，提供功能與生理性訊息，代謝產物 NAA 訊號下降表示大腦的神經組織受損，在正常情況下，它的存在表示神經元和軸突的完整性。擴散權重影像 (Diffusion-weighted image; DWI) 越來越多應

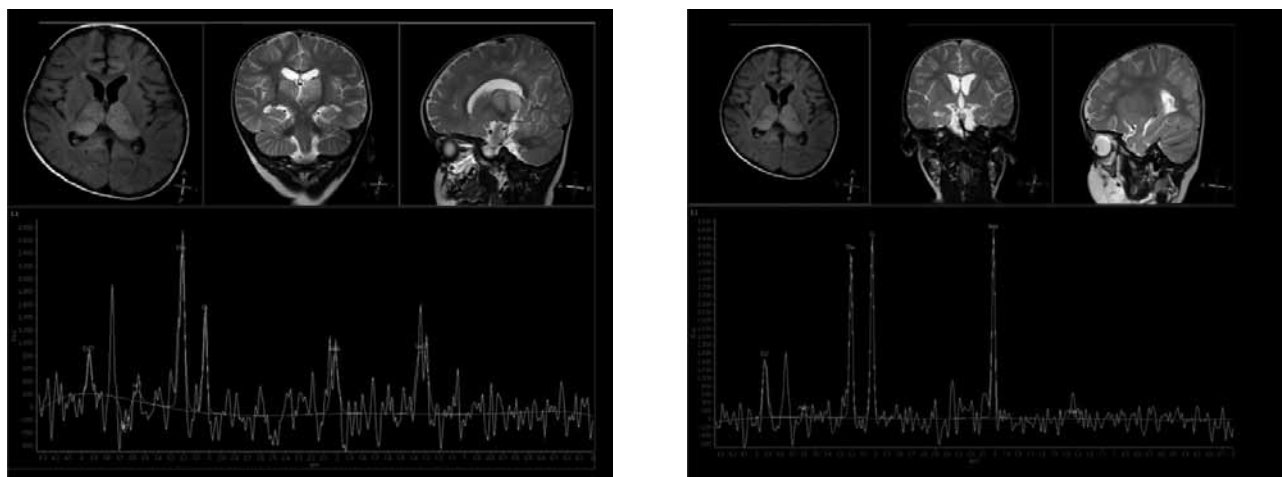


圖 1 腦部 MRI (axial view) 顯示，在 T2 影像雙側腦丘、左側尾核、黑質及腦迴頭尾均有高訊號與細胞毒性水腫，MRS 顯示乳酸出現減少了 NAA 訊號。

註 1：成對血清各經序列稀釋 (1:100, 1:200, 1:400, 1:800)，由 ELISA OD 值比較是否有四倍上升。本案例一採檢體 1:100 的 OD 值為 0.275，二採檢體 1:400 的 OD 值大於 0.275，有 4 倍增加。

用於各種的大腦疾病，可檢測各種病毒性和細菌性腦炎的早期病變。DWI 與表觀擴散係數 (apparent diffusion coefficient; ADC) 對於日本腦炎的病程有顯著的直接關係。在急性期，血管周圍圍管現象和充血導致局部缺血及細胞毒性水腫，而限制擴散與低 ADC；在亞急性期，限制擴散比率減少，ADC 開始上升；在慢性期，壞死和脫髓鞘是低信號 DWI 和較高 ADC 的原因 [12]。

在治療方面並無特殊的抗病毒藥物 [3]，主要為支持性療法，最重要為控制腦壓，其他方面如控制發燒及抽搐、注意體液平衡、呼吸器支持、預防及治療次發性感染，若支持療法得宜，可提升存活，改善預後。日本腦炎的診斷包括季節性、居住地區、流行地區工作或旅遊史、蚊蟲叮咬、疫苗接種、臨床表徵、血清學檢查與腦部 MRI 檢查等，而典型之腦部 MRI 特徵將有助於早期診斷 [7,11-14]。因日本腦炎為具潛在致命性但可預防之傳染性疾病，所以疫苗接種是最好的預防方法，另外環境公共衛生以及避免蚊蟲叮咬，也是很重要的預防措施。

參考文獻

1. 許麗卿、吳盈昌、何美鄉、林雪蓉、盧志對、陳國東等人：臺灣鄉村地區 3-6 歲兒童日本腦炎病毒感染的血清流行病學調查。疫情報導 1995；11：229-239。
2. 行政院衛生署疾病管制局：傳染病統計資料查詢系統 (民 100)。[Online]. Available : http://nidss.cdc.gov.tw/NIDSS_report.aspx?pt=s&Dc=2&Dt=4&disease=0620&d=3&s=determined_cnt&i=all&RK=Y
3. Misra UK, Kalita J: Overview: Japanese encephalitis. *Prog Neurobiol* 2010 Jun;91:108-120.
4. Shu PY, Chen LK, Chang SF, Yueh YY, Chow L, Chien LJ, Chin C, Lin TH, Huang JH. Comparison of capture immunoglobulin M (IgM) and IgG enzyme-linked immunosorbent assay (ELISA) and nonstructural protein NS1 serotype-specific IgG ELISA for differentiation of primary and secondary dengue virus infections. *Clin Diagn Lab Immunol*. 2003;10:622-30.
5. Abe T, Kojima K, Shoji H, Tanaka N, Fujimoto K, Uchida M et al: Japanese encephalitis. *J Magn Reson Imaging* 1998;8: 755-761.
6. Solomon T, Dung NM, Kneen R, Gainsborough M, Vaughn DW, Khanh VT: Japanese encephalitis. *J Neurol Neurosurg Psychiatry* 2000;68:405-415.
7. Kalita J, Misra UK: Comparison of CT scan and MRI findings in the diagnosis of Japanese encephalitis. *J Neurol Sci*. 2000;174:3-8.
8. Cagatay AA, Ozsut H, Gulec L, Kucukoglu S, Berk H, Ince N, et al. Tuberculous meningitis in adult-experience from Turkey. *Int J Clin Pract* 2004;58:469-473.
9. Kumar S, Misra UK, Kalita J, Salwani V, Gupta RK, Gujral R. MRI in Japanese encephalitis. *Neuroradiology* 1997;39: 180-184.
10. Chen KM, Tsai HC, Sy CL, Lee SS, Liu YC, Wann SR, et al: Clinical manifestations of Japanese encephalitis in southern Taiwan. *J Microbiol Immunol Infect*. 2009;42:296-302.
11. Lai CC, Liu WL, Lin SC, Hsiao YC, Ding LW: Diagnostic MR images of Japanese encephalitis. *J Emerg Med* 2008;35: 305-307.
12. Chen WP, Leung JH, Ng YB, Huang CL: Magnetic resonance imaging features in Japanese encephalitis: two cases report. *Clin J Radiol* 2005;30:347-351.
13. Yip JS, Chen CM. Magnetic resonance image findings in four patients with Japanese encephalitis. *J Emerg Crit Care Med* 2007;18:110-114.

Case Report of Magnetic Resonance Imaging Findings Japanese Encephalitis

Chung-Chih Kao^{1*}, Chia-Ru Li², Ching-Shiang Chi¹, Ai-Min KuLiu¹,
Stella Chin-Shaw Tsai^{2,3}, Chia-Hui Kao¹

¹Department of Pediatric, ²Department of Medical Research, the ³Department of Otolaryngology,
Tungs' Taichung MetroHarbor Hospital, Taichung, Taiwan

Received: May 28, 2013; Accepted: Aug. 23, 2013

ABSTRACT

Japanese encephalitis is an important cause of viral encephalitis in East and South Asia. Here we report the case of a 16-month-old boy presenting with a 7-day history of cough and runny nose, accompanied by fever. On clinical presentation, he developed repetitive general spasms and unconsciousness. A 4-fold increase was detected in serum immunoglobulin M antibody titers for Japanese encephalitis virus. Diagnosis of Japanese encephalitis was confirmed on the basis of several factors: seasonality, location, work or travel within endemic areas, mosquito bites, vaccination history, clinical features, serology, and brain magnetic resonance imaging (MRI). These findings suggest that when a patient with suspected Japanese encephalitis develops fever, headache, and a change in consciousness, typical hypothalamic lesions identified on brain MRI can clarify the diagnosis. Currently, Japanese encephalitis vaccination is the most direct and effective method of preventing this disease.

Key word: Japanese encephalitis, MRI



謹向2013年童綜合醫學雜誌審查者致謝

(依姓氏筆劃排列)

王德明

朱本元

朱永祥

吳百堯

吳昌杰

李孟訓

余慕賢

呂志成

沈俊佑

林岑蔚

林志堅

周啟文

金忠孝

洪至仁

洪豪駿

姜仁惠

唐友文

唐國民

許弘毅

許志宏

陳世宜

陳明哲

陳伯彥

張立偉

廖文進

劉錦成

劉益瑞

劉時安

鄭聖翰

蔡青劭

錢新南

謝財源

Instruction to contributors

This journal provides a forum for medical related articles, such as original researches, clinical analysis, case reports and special review articles, special articles, communication (includes brief communication), images in clinical medicine, editorial and etcetera. Manuscripts should be submitted to the editorial board of Tungs' Taichung MetroHarbor Hospital Medical Journal: ADD:No.699, Sec.8, Taiwan Blvd., Wuqi Dist., Taichung City 43503, Taiwan (R.O.C)
E-mail: Tungs_journal@ms.sltung.com.tw

Submission of Manuscripts:

1. The manuscript is required in duplicate (includes an original manuscript and a copy of the original manuscript, however, figures/legends need two original copies) alone with an electronic copy of the latest version; please do not staple the document, if electronic file of figures and/or pictures is being provided, please attached as a JPG format.
2. The content of the document need to be clear, and is consistent with the original copy, the author need to be responsible if the duplicate is different from the original copy or is missing. If the content is related to copyright, author needs to obtain the right to use and is legally responsible for it.
3. Please attached the copyright and consent form on submission. All author(s) listed must actually participate in and agree with the conclusion. Upon receiving and completion of printing, the author(s) will receive 20 free copies and compensation. If extra copy is needed, please notify during editing, and this is subjected to charges.
4. After acquiring consent from the author(s), author(s) agreed to any editing. The submission is returnable, if any, when the manuscript is incompatible with the journal's mission.
5. For any articles listed on the journal, please follow the protocol if related to "the collection of human specimen for research" and "human clinical trail" to ensure the right of participants
6. If the article is related to the use of vertebrates for science application, the project need to be verified by associated animal laboratory management team to ensure the humane management for laboratory animals.

Principles of writing:

1. Original article should be arranged by the following sequence: abstract, introduction, material and methods, results, discussion and conclusion, acknowledgements, reference, attachments, figures and legends for illustration.
2. Case report should be arranged by the following sequence: abstract, introduction, clinical records, discussion, reference, attachments, table, figures and legends for illustration. Each note should be no longer than 5 pages and should be written with the following order: topic, organization, the name of author(s), past history and critical diagnosis, primary clinical problem,

discussion or analysis, conclusion, and references. Patients' eyes should be covered in the picture for privacy. Diagnosis information or the chart of clinical process should be within 6 months.

3. There is no regular form for review articles, but references need to be listed.
4. Images in clinical medicine should be arranged by the following sequence: abstract, figures and legends for illustration.
5. Other types of article should be no longer than 4 pages including charts, except for articles with special arrangement.
6. For other details, please refer to international steering committee, for uniform requirements for manuscripts submitted to biomedical journals please refer to The New England journal of medicine 336:309-315,1997.

Manuscript preparation:

Manuscript should be double-spaced and numbered pages, and comply with the "uniform requirements for manuscripts submitted to biomedical journals". The first page is the title page, which include title, name of author(s), organization and unit, contact name, phone number and address (in both Chinese and English). The second and the third page is for abstract (Chinese content needs to consist with English content) and key words (please include 3 to 5 keywords or phrases in Chinese and English), and should be written in paragraphs following by background and purpose, methods, results and discussion.

Co-corresponding author should mention the contributions on manuscript, such as initiation of research topics, the study design, statistical analysis, interpretation of findings, chapters writing involved et al.

Please attach two original copies including attachments, charts and legends. Chart should be professional, with only one figure or one table per page, and is arranged in consecutive orders and numbered in Arabic characters. Table should have a title and appropriate interpretation. Picture should be 5"x 7" in size, black and white, glossy and numbered in consecutive orders of appearance.

Reference:

Unpublished articles or abstracts cannot be listed as references, but could be noted as "unpublished observations". Doctoral dissertation or master thesis can be used. Any articles being accepted by magazines but not published yet, please note the name of magazine, year and note "in press".

Original research, clinical analysis, case reports and special review articles follows the following format:

1. Abbreviations used should follow the format of Index Medicus for all journal titles. When authors are less than 6 people, list all author(s), when more than 6, only list the first 6 followed by "et al" for the rest.

2. References in the text should be placed where relevant. When a reference article is cited, only the primary author is cited; however, if only two authors are present, both should be listed.
3. Example of references:

Examples of Reference:

1. Periodicals:

Yang KTA, Chen HD: A semi-automated method for edge detection in the evaluation of left ventricular function using ECG-gated single-photon emission tomography. Eur J Nucl Med 1994;21:1206-11.

2. Monographs:

Plum F, Posner JB: Diagnosis of Stupor and Coma. 3rd ed. Philadelphia: Davis, 1980:132-3.

3. Monographs with multiple authors:

Levinsky NG: Fluid and electrolytes. In: Thorn GW, Adams RD, Braunwald E, Isselbacher K, Petersdprf RG eds. Harrison's Principles of Internal Medicine, 8th ed. New York: McGraw-Hill, 1977:364-75.

Copyright:

If any submission being accepted by Tungs' Taichung MetroHarbor Hospital Medical Journal, the author(s) agree to grant the Medical Journal the right to sublicense the National Central Library or any other database providers to reproduce, transmit publicly by internet, download, print and browse by authorized users. The submission may be changed to meet the requirement of databases.

童綜合醫學雜誌投稿相關規則

95.9.01 製訂
99.08.17 修訂
100.07.11 修訂
102.07.08 修訂
102.12.27 修訂

本雜誌刊載與醫學有關之論述，包括原著論文、病例分析研究、病例報告等論述及特別約稿之綜論 (review article)、special article、communication (包括 brief communication)、影像判讀、Editorial (編著的話) 等。惠稿請送 43503 臺中市梧棲區臺灣大道八段 699 號童綜合醫學雜誌編審委員會。(E-mail:Tungs_Journal@ms.sltung.com.tw)

壹、投稿前注意事項

1. 投稿時，需附原稿兩份（一份原稿和一份複印稿，但圖片應用兩份原圖）並以電腦打字（請以 MS WORD 文書處理格式，中文字型以標楷體，英文字型以 Time New Roman 12 號字大小，稿紙之左右緣為 2.54 公分，上下緣為 3.17 公分），請勿裝訂，同時須提供最後版本之電子檔一份，若圖片或照片有電子檔提供者，請以附檔 jpg 的形式提供。
2. 文件內容需清晰，內容與原稿一致，若複印稿與原稿有差異或遺漏，由作者自行負責。著作中若牽扯到版權所有之內容，作者需取得其使用權，法律責任由作者負責。
3. 投稿同時請附上著作權讓與同意書。所有作者必須實際參與並同意該論述。本院於接受稿件且印刷完成後，將致贈稿酬並贈送 20 份抽印本給通訊作者，如需額外抽印本請於校稿時言明，並酌收成本費用。第一作者若需抽印本可提出申請，依份數酌收成本費用。
4. 本刊對於原稿經徵得著者之同意得伸縮或修改之。如不合本刊宗旨者，得退還之。
5. 凡刊載於本雜誌之著作，若涉及「研究用人體檢體採集」及「人體試驗」等情事，應遵守該注意事項，以落實保障受檢人權益。詳文請參考須附上相關審議認可之文件。
6. 論文中如涉及使用脊椎動物進行科學應用計畫者，應檢附該計畫業經所屬機構動物實驗管理小組審議認可之文件，以落實實驗動物之人道管理。

貳、寫作原則

1. 原著論文按下列順序撰寫：摘要、前言、材料與方法、結果、討論與結論、誌謝、參考文獻、附表、圖片說明、圖片（含照片）。
2. 病例報告按下列順序撰寫：摘要、前言、病例、討論、參考文獻、附表、圖片說明、附圖、照片。
3. 病例報告，每篇以五頁以內為限（即約 9,000 字），依題目、所屬機構、作者姓名（作者以 5 人為限）、病例之病史經過及重要之診療資料、主要之臨床問題、討論或分析、結論、推薦讀物等順序繕寫。凡病患顏面部之相片必須遮去眼睛部位，表示尊重隱私。診療資料或臨床經過之圖表，原則上均限六個月以內。
4. 綜說不必按原著論文格式撰寫，但必須列出參考文獻。
5. 影像判讀按下列順序撰寫：摘要、圖例說明。
6. 其他類文章連圖表，以不超過四頁（每頁約 2,000 字）為原則，但特約稿例外。
7. 其他細節，請參閱國際指導委員會（International Steering Committee）發表之生物醫學雜誌稿件統一規格（Uniform Requirements for Manuscripts Submitted to Biomedical Journals，見 The New England Journal of Medicine 336:309-315,1997）。

參、投稿須知

1. 稿件須符合「生物醫學雜誌投稿之統一規定」1，請以電腦隔行 double space 書寫並編頁碼。
2. 第一頁為標題頁，須列出中文及英文之論文題目、中英文作者姓名、所屬機構及單位之中英文稱號（分屬不同單位，請以阿拉伯數字標出作者與單位）、聯絡人姓名、電話及中英文通訊錄。

3. 第二、三頁為中文及英文之摘要及關鍵詞（請提供3至5個關鍵詞或簡短片語），中英文摘要須完全相同，摘要分段撰寫，依序為背景及目的（Background and purpose）、方法（Methods）、結果（Results）及討論（Discussion）。
4. 相同貢獻作者請加註說明，如研究主題的設定、參與決定研究設計、進行統計分析、詮釋研究結果、以及各章節撰稿等貢獻。
5. 請附兩份原稿（一份原稿和一份複印稿，但圖片應使用原圖），包括附表、附圖及照片。圖表應專業製作，一張紙僅一個附圖或附表，依引用順序以阿拉伯數字標出排列。附表須有標題及說明。照片須5×7吋光面黑白，背面以鉛筆編號，附圖須有簡單說明（Legend），並另頁撰寫。光學或電子顯微鏡照片，請註明擴大倍率或比例。

註：¹ 根據「生物醫學雜誌投稿之統一規定」第五版，刊載於 *Annals of Internal Medicine* 1997;126(1): 36-47.

肆、參考文獻

未經發表之論文或摘要不得列為參考文獻，但可於本文中說明並註明「未發表」（unpublished observations）。博碩士論文可引用。已被任何雜誌接受刊發但仍未發表之著作，請列出雜誌名稱及年份，並註明「in press」。

原著論文、病例分析研究、病例報告等論述及特別約稿之綜論（review article）按下列格式撰寫：

1. 雜誌名稱之簡稱須按照 Index Medicus 型式，作者人數小於6位時，詳列所有作者姓名，超過6位時，只須列出前6位，其它以「等」（et al）代替。

例：Bhasin S, Storer TW, Berman N, Callegari C, Clecenger B, Phillips J, et al. The effects of supraphysiologic doses of testosterone on muscle size and strength in normal men. *N Engl J Med* 1996; 335:1-7.

2. 本文內引用時，若兩名以下作者請列出姓氏。兩名以上則列出第一名之姓氏，其他以「等」（et al）代替，並以阿拉伯數字方括弧表示於引用之後。

例：One of the first well documented reports of ECH poisoning with fatality in young children was reported by Miller et al. in 1970[2].

例：Boulet 等人 [3] 報告氣喘患者接受衛教後的知識改變量不受個人因素影響

3. 參考範例

A. 期刊：[作者姓名：題目。雜誌簡稱 年代；卷數（期數）：起迄頁數]

(1) 許吟姿、楊光道、張恆鴻：結締組織疾病併發間質性肺病變患者 99mTc-DTPA 肺廓清率之臨床研究。內科學誌 1992;3:79-83.

(2) Yang KTA, Chen HD: A semi-automated method for edge detection in the evaluation of left ventricular function using ECG-gated single-photon emission tomography. *Eur J Nucl Med* 1994;21:1206-11.

B. 單行本：[作者姓名：書名，版數（卷數）。發行地；出版公司，年代：引用部份頁數]。

(1) 楊志良：生物統計學新論，一版。台北；巨流圖書公司，1984：33-8.

(2) Plum F, Posner JB: *Diagnosis of Stupor and Coma*. 3rd ed. Philadelphia: Davis, 1980:132-3.

C. 多重作者之單行本：[有關文章作者姓名：書名，版數（卷數）。發行地；出版公司，年代：引用部份頁數]。

(1) 蔣欣欣：護理與健康，編輯：顧乃平：護理專業導論，一版。台北；匯華出版公司，1991：83-121。

(2) Levinsky NG: Fluid and electrolytes. In: Thorn GW, Adams RD, Braunwald E, Isselbacher K, Petersdprf RG eds. *Harrison's Principles of Internal Medicine*, 8th ed. New York: Mcgraw-Hill, 1977:364-75.

伍、著作權

若著作人投稿於本刊經收錄後，同意授權本刊得再授權國家圖書館或其他資料庫業者，進行重製、透過網路提供服務、授權用戶下載、列印、瀏覽等行為。並得為符合各資料庫之需求，酌作格式之修改。若為摘譯、譯稿或改寫稿，需附原作者之正本同意書，並附原文影本一份；來稿如涉及版權，概由作者自負文責。

童 綜 合 醫 學 雜 誌

綜 論

- 37 抗血管新生藥物在卵巢上皮癌的臨床實驗回顧
劉錦成

原 著

- 44 比較窄頻影像及傳統白光影像在區別大腸息肉之診斷表現
蔡明宏 沈偉誌
- 59 蘋果多酚在動物模式中抑制脂多醣誘導之發炎作用
李慧禎

病例報告

- 66 在插管式全身麻醉下移除巨大的卵巢腫瘤時出現渡過性血氧飽和度下降：病例報告
陳耀舜 黃國生 張錦新 文寄銘 馬振來 簡陳榮
- 70 腰椎痛風性關節炎：一病例報告
李心白 劉思源 謝時鵬 施承貴 簡言軒
- 76 以核磁共振早期診斷日本腦炎之病例報告
高崇智 李佳茹 遲景上 古劉愛敏 蔡青劭 高佳慧

ISSN 2071-3592

童 綜 合 醫 學 雜 誌

中華民國九十六年十二月創刊
預定出版日期：每年六、十二月三十日出刊

發行人：童瑞年

總主編：張子明

編輯顧問：陳穎從 殷約翰

副總編輯：遲景上 許弘毅 廖文進 童瑞文

執行編輯：鄒順生

編審委員：

尹裕君	王朝鐘	何家爽	李秀芬
李慧禎	林柏松	林岑蔚	林敬恆
林肇堂	金忠孝	俞志誠	查岱龍
姜仁惠	徐少克	陳宗勉	陳培亮
陳得源	曹唐義	曾志仁	童敏哲
黃瑞芬	葉坤土	葉庭瑜	潘品合
蔡青劭	鄭啟清	劉錦成	盧星華
謝良博			

(依姓氏筆劃排列)

統計顧問：鄭雅中

法律顧問：林松虎 黃清濱

編輯助理：王孟怡 易美慧

出版編輯部：

童綜合醫學雜誌編審小組

地址：43503 臺中市梧棲區臺灣大道八段 699 號

E-Mail：Tungs_Journal@ms.sltung.com.tw

Tel：〈04〉26581919 ext 58047

Fax：〈04〉26582193

印刷者：

大光華印務部

地址：10851 台北市萬華區廣州街 32 號 6 樓

Tel：〈02〉2302-3939 (代表號)

Fax：〈02〉2302-2036